A posteriori error estimates and adaptive stopping criteria for cardiac monodomain model

Fakhrielddine Bader*†   Jad Dabaghi‡   Hala Ghazi§

June 25, 2025

Abstract

In this work, we consider the monodomain problem to simulate the electrical activity within the heart tissue. From a mathematical standpoint, it is modeled by a nonlinear parabolic partial differential equation coupled with an ordinary differential equation, whose numerical resolution is often challenging and computationally expensive. We employ the backward Euler scheme for the time discretization and the conforming $\mathbb{P}_p$ finite element method for the spatial discretization. We derive a guaranteed *a posteriori* error estimate on the error between the exact solution at the continuous level and the approximate solution that is valid at each time step and each iteration of the linearization solver. Our estimate, based on equilibrated flux reconstructions, also distinguishes the spatial and temporal components of the error. The spatial component further consists of the discretization error and the linearization error. At each time step of the simulation, we propose an adaptive version of the Newton algorithm based on stopping the Newton iterations when the estimators of the corresponding error components does not affect significantly the overall estimate. In addition, this adaptive procedure leads to computational savings while ensuring the accuracy of the solution. Numerical experiments are presented to demonstrate the effectiveness of the proposed approach.

Keywords: Monodomain model; Reaction-diffusion system; The finite element method; A *posteriori* error estimates; Adaptivity; Cardiac electrophysiology.

1 Introduction

The study of the electrical activity of the heart generates broad interest among researchers and clinicians who are concerned with the understanding and the development of therapies for complex chronic diseases. This subject is of fundamental importance in biomedical sciences since experiments on living hearts provide only a partial picture of the heart's electrical activity. The mathematical modeling of the electrical activity of the heart [43, 63] has received significant attention over the past decades and constitutes one of the most important applications in life science. These models are used to study various aspects of the electrical activity in the cardiac tissue to identify dysfunctions such as heart rhythm disorders in the atria and mechanisms of defibrillation. One of the most accurate descriptions of the electrical cardiac behavior is given by the so-called "bidomain model" [22, 37, 63]. We also mention the "extracellular-membrane-intracellular" (EMI) or "tridomain" model [67, 42, 9, 10] that describes the electrical activity of myocyte cells in the presence of gap junctions. Compared to the bidomain model, the cells are not only electrically coupled by the cell membranes, which are resistively connected to the extracellular space, but are also connected to each other via numerous gap junctions.

Established by Schmitt [61] and first formally developed by Tung [66], the bidomain formulation models an active myocardium at the macroscopic scale. This model consists of two partial differential equations (PDEs) modeling the intra- and extracellular potentials. The PDEs are coupled with a system of ordinary

---

*IHU LIRYC Institute, Fondation Université de Bordeaux, Pessac, France
†Institute of Mathematics of Bordeaux, UMR 5251, University of Bordeaux, Talence, France
‡Léonard de Vinci Pôle Universitaire, Research Center, 92 916 Paris La Déefense, France
§Icam School of Engineering, Nantes Campus, 35 Avenue du Champ de Manoeuvres, Carquefou 44470, France

differential equations (ODEs) describing the ion currents across the membrane. A complete derivation of this macroscopic model directly from the microscopic properties of the cardiac tissue, using asymptotic and homogenization methods along with basic physical principles, is presented in [39, 4, 7, 8] for the bidomain model and in [9, 10] for the tridomain model. Assuming that anisotropy ratios between intracellular and extracellular media are equal, we obtain a simplification of the bidomain formulation known as the monodomain model. From a mathematical standpoint, the monodomain formulation consists of a nonlinear parabolic PDE describing the transmembrane voltage, which is defined as the difference between the intra- and extracellular potentials, coupled with a system of ODEs representing the ionic dynamics, see also [22, 37, 65] and the references therein. Unfortunately, deriving an analytical solution for the monodomain model is often out of reach, and numerical simulations seem to be the only viable approach to approximate a solution. The development of numerical methods for solving complex systems of PDEs has been a very active field of research in the past. We mention the well-known and rooted finite element method [54, 18, 14], the finite volume method [34, 41, 35], or the discontinuous Galerkin method [5, 57, 28]. Some recent contributions about hybrid high-order (HHO) methods have been introduced in the literature, see [29, 23].

Concerning more specifically the monodomain formulation, several numerical approaches have been proposed to address its computational challenges. We mention first the explicit stabilized multirate methods that have proven to be efficient for solving the nonlinear monodomain equation. These methods leverage local time-stepping and multirate techniques to handle the fast dynamics of depolarization waves while circumventing stringent stability constraints associated with mesh refinement [59]. Another promising approach involves operator splitting techniques, where the PDE is decomposed into its reaction and diffusion components. Examples include the first-order Godunov method [64] and the second-order Strang splitting method [53], both of which have shown to improve computational efficiency and accuracy. Furthermore, advanced time-splitting schemes have been developed to efficiently approximate the rapid depolarization dynamics. These schemes separate the fast and slow components of the monodomain equations, facilitating scalable computations for large-scale simulations of cardiac electrical activity [44].

Some fundamental questions arise in the numerical simulation of such systems. Can we estimate the error and where is it localized ? Can we estimate separately the different error components of the numerical scheme? To address these points we perform an a posteriori analysis of the monodomain formulation relying on equilibrated flux reconstruction including adaptive stopping criteria for nonlinear solvers.

A significant amount of work has been carried out in the last years on a posteriori analysis of PDEs (see for instance the books of Verfürth [69], Ainsworth and Oden [2] and Repin [56] for a general introduction) where the goal is to derive a guaranteed fully computable upper bound for the error in a certain norm. These estimates differ from the traditional a priori error estimates in which the upper bound on the error depends on the unknowns of the problem. We mention the pioneering references [19, 62, 17] and also Sanfelici [60] in the context of electrocardiology. In the context of parabolic problems, the a posteriori analysis mainly focused on the $\mathbb{P}_1$ finite element discretization in space coupled with an implicit Euler or Crank–Nicolson time-stepping scheme. In general, the estimate is performed on the discretization error. We mention for instance the contributions of Verfürth [68] or Bernardi, Bergham, and Mghazli [13]. We also emphasize on the recent survey of [30], in which local efficiency in space and time for the estimators is also proven. Other works explored the construction of a posteriori error estimates not only on the discretization error but also at each nonlinear or linear steps employed through the simulation. These works are based on locally conservative H(div)- conforming reconstruction of the flux, piecewise constant in time. This equilibrated reconstruction of the flux follows the concept of Destyunder and Métivet [26], Braess, and Schöberl [16], Dabaghi eal [24, 38, 25], Ern and Vohralík [32]. An attractive feature of this approach is that it is suitable for a unified setting: the a posteriori error analysis does not rely on the underlying discretization scheme compared to other approaches such as residual based a posteriori error estimates (see [69] and the references therein). This method in particular leads to an adaptive procedure in which the iterations of the underlying solvers are stopped whenever the corresponding errors drop to the level at which they no longer significantly affect the overall error. We refer to the pioneering studies of [27, 11] and the recent works of [24, 32] for elliptic problems and [25, 38] for parabolic and industrial problems.

Concerning a posteriori error estimates for monodomain formulation, few works have been addressed in the literature to the best of our knowledge. Luca and Verani [55] employed the $\mathbb{P}_1$ finite element method and established residual-based a posteriori error estimates, including space-time and linearization indicators. Their approach provides a guaranteed upper bound on the $L^2(H^1)$ error norm with a reliability constant depending on the mesh. Chellappa et al. [20] introduced fast reduced-order models integrated with a

posteriori error estimators to refine parameter spaces and improve computational efficiency in large-scale simulations. Similarly, Mirabella et al. [47] proposed a hybrid bidomain-monodomain model coupled with a posteriori error control to reduce computational costs. Next, in [21] and [6], the authors employed space-time adaptivity using a posteriori error estimators on the discretization error to dynamically refine spatial meshes and time steps.

In our work, we employ a high-order finite element method and the methodology of equilibrated flux reconstruction so as to obtain a fully computable bound on the error at each linearization solver step and to derive an adaptive procedure so as to save unnecessary iterations. We also emphasize on the fact that our methodology produces a reliability constant equal to 1.

The present work paper is structured as follows. In Section 2, we present the monodomain problem and its weak formulation. Next, in Section 3, we introduce its discretization with the implicit Euler scheme in time and the conforming $\mathbb{P}_p(p \geq 1)$ finite element method in space. Then, we present the Newton algorithm to approximate the solution of our nonlinear system at each time step. Furthermore, Section 4 is devoted to the a posteriori analysis following the approach of the equilibrated flux reconstructions. Therefrom, in Section 5 we propose an adaptive version of our Newton method based on the distinction of the error components, namely the discretization error and the linearization error. Finally, Section 6 reports some numerical experiments, assessing the strengths of our approach.

2 Monodomain modeling of the heart tissue

In this section, we set up the notation, describe in detail the monodomain model, and introduce its finite element discretization for all polynomial degrees $p \geq 1$.

2.1 Monodomain model and setting

We consider a bounded, open, polygonal, connected domain $\Omega \subset \mathbb{R}^d$, $d = 2, 3$, with Lipschitz boundary $\partial\Omega$. We denote by $T > 0$ the final simulation time, and we set $\Omega_T := (0, T) \times \Omega$. Let $\mathcal{D}(\Omega)$ be the space of $\mathcal{C}^\infty$ functions with compact support on Ω and $\mathcal{D}'(\Omega)$ its dual version. Let $H^1(\Omega)$ be the space of L^2 functions on the domain Ω which admit a weak gradient in $L^2(\Omega)$ and $H_0^1(\Omega)$ its zero-trace subspace. The duality pairing between any Sobolev space V and its dual space V' is denoted by $\langle \cdot, \cdot \rangle_{V', V}$. Similarly, $\mathbf{H}(\text{div}, \Omega)$ stands for the space of $\left[L^2(\Omega)\right]^d$ functions having a weak divergence in $L^2(\Omega)$. The standard notations $\boldsymbol{\nabla}$ and $\boldsymbol{\nabla}\cdot$ are used respectively for the weak gradient and divergence operators. For a nonempty set $\mathcal{O}$ of $\mathbb{R}^2$, we denote its Lebesgue measure by $|\mathcal{O}|$ and the $L^2(\mathcal{O})$ scalar product by $(u, v)_{\mathcal{O}} := \int_{\mathcal{O}} uv \, \text{dx}$ for $u, v \in L^2(\mathcal{O})$. We also use the following notations: $\|v\|_{\mathcal{O}}^2 := (v, v)_{\mathcal{O}}$, and $\|\boldsymbol{\nabla} v\|_{\mathcal{O}}^2 := (\boldsymbol{\nabla} v, \boldsymbol{\nabla} v)_{\mathcal{O}}$. Besides, the Poincaré-Friedrichs and the Poincaré-Wirtinger inequalities, see [1], state that if $\bar{v}_{\mathcal{O}}$ denotes the mean value of v and $h_{\mathcal{O}}$ the diameter of $\mathcal{O}$, then

$$\|v\|_{\mathcal{O}} \leq C_{\text{PF}} h_{\mathcal{O}} \|\boldsymbol{\nabla} v\|_{\mathcal{O}} \quad \forall v \in H_0^1(\mathcal{O})$$
$$\|v - \bar{v}_{\mathcal{O}}\|_{\mathcal{O}} \leq C_{\text{PW}} h_{\mathcal{O}} \|\boldsymbol{\nabla} v\|_{\mathcal{O}} \quad \forall v \in H^1(\mathcal{O}).$$

The constants C_{PF} and C_{PW} can be precisely estimated in many cases. In particular, if $\mathcal{O}$ is convex, C_{PW} can be taken as $\frac{1}{\pi}$, see [1] whereas C_{PF} is at most 1.

We consider the monodomain model:

$$\begin{aligned}
\partial_t v - \boldsymbol{\nabla} \cdot (\Lambda \boldsymbol{\nabla} v) + f(v, w) &= 0 && \text{in } \Omega_T, \\
\partial_t w + g(v, w) &= 0 && \text{in } \Omega_T, \\
\Lambda \boldsymbol{\nabla} v \cdot \boldsymbol{n} &= 0 && \text{on } (0, T) \times \partial\Omega, \\
v|_{t=0} = v^0, \quad w|_{t=0} &= w^0 && \text{in } \Omega.
\end{aligned} \tag{2.1}$$

In System (2.1), the unknown variables are the transmembrane potential $v(t, \boldsymbol{x}) \in \mathbb{R}$, and the ionic variable $w(t, \boldsymbol{x}) \in \mathbb{R}$ (gating variable, concentration, etc) which is an auxiliary function characterizing the underlying transfer of ions across the membrane in the considered medium. The first line of (2.1) describes

the balance of current in the heart muscle where $\partial_t v$ is the capacitive current, $\boldsymbol{\nabla} \cdot (\Lambda \boldsymbol{\nabla} v)$ is the ohmic current, and $f(v, w)$ is the ionic current induced by the cellular activation. In this model, the anisotropic characteristics of the tissue are given by the tensor $\Lambda(\boldsymbol{x}) \in \mathbb{R}^{d \times d}$. The second line of (2.1) describes the dynamic of the activation and inhibition variables for the ionic channels and $g(v, w)$ is a function representing the ionic activity. In an isolated heart, no current flows out of the heart, as expressed by the boundary condition (third line of (2.1)) where $\boldsymbol{n}$ is the outward unit normal vector to $\partial \Omega$. Finally, the last line of (2.1) corresponds to the initial conditions for the functions v and w.

Assumption 2.1 (Assumptions on the conductivity tensor)**.** *Assuming an anisotropic medium, the conductivity is represented by the tensor $\Lambda(\boldsymbol{x})$ (with coefficients in $L^\infty(\Omega)$) which is a symmetric, bounded, and uniformly positive definite on Ω. It means that*

$$\exists (m_0, M_0) \in \mathbb{R}_+^* \times \mathbb{R}_+^* \ s.t \ \forall \boldsymbol{\xi} \in \mathbb{R}^d, \ 0 < m_0 \left| \boldsymbol{\xi} \right|^2 \leq \Lambda \boldsymbol{\xi} \cdot \boldsymbol{\xi} \leq M_0 \left| \boldsymbol{\xi} \right|^2 .$$

Assumption 2.2 (Assumptions on the ionic functions)**.** *The total ionic current f in the first line of (2.1) can be decomposed as $f(v, w) = f_1(v) + f_2(w)$ where the nonlinear function $f_1 : \mathbb{R} \to \mathbb{R}$ is considered as a C^1 function and the functions $f_2 : \mathbb{R} \to \mathbb{R}$ and $g : \mathbb{R}^2 \to \mathbb{R}$ are considered as linear functions. Also, we assume that there exists $r \in (2, +\infty)$ and constants $\alpha_i > 0$ $(i = 1, \ldots, 5)$, and $\beta_j > 0$ $(j = 1, 2)$ such that:*

$$\frac{1}{\alpha_1} |v|^{r-1} \leq |f_1(v)| \leq \alpha_1 \left(|v|^{r-1} + 1 \right), \quad |f_2(w)| \leq \alpha_2(|w| + 1), \tag{2.2a}$$

$$|g(v, w)| \leq \alpha_3(|v| + |w| + 1), \ \text{and} \ f_2(w)v + \alpha_4 g(v, w)w \geq \alpha_5 |w|^2 , \tag{2.2b}$$

$$\tilde{f}_1 : v \mapsto f_1(v) + \beta_1 v \ \text{is strictly increasing with} \ \lim_{v \to 0} \tilde{f}_1(v)/v = 0, \tag{2.2c}$$

$$\forall (z_1, z_2) \in \mathbb{R}^2, \ \left(\tilde{f}_1(z_1) - \tilde{f}_1(z_2) \right) (z_1 - z_2) \geq \frac{1}{\beta_2} (1 + |z_1| + |z_2|)^{r-2} |z_1 - z_2|^2 . \tag{2.2d}$$

Remark 2.3. *In the mathematical analysis of monodomain equations, several paths have been addressed in the literature according to the definition of ionic currents. To fix the ideas, we present two common approaches for constructing these ionic models in cardiac simulation: the phenomenological and physiological models. The first one simplifies the underlying mechanisms and focuses on reproducing characteristic behaviors (such as ventricular dynamics) at the macroscopic scale. In terms of computational cost, these models are competitive but unfortunately do not capture the entire physical processes. One of the most well-known phenomenological model is the FitzHugh–Nagumo model [36, 49]. This model is often studied because it is analytically tractable and satisfies Assumptions 2.2 where*

$$g(v, w) = -av + bw, \tag{2.3a}$$
$$f(v, w) := f_1(v) + f_2(w) \tag{2.3b}$$

with

$$f_1(v) := \lambda v(v - 1)(v - \theta) \quad \text{and} \quad f_2(w) = \lambda w$$

and a, b, λ, θ are given parameters satisfying $a \geq 0$, $b \geq 0$, $\lambda > 0$ and $0 < \theta < 1$. We mention other phenomenological ionic models: the Roger-McCulloch model [58], the Aliev-Panfilov model [3], and the Mitchell-Schaeffer model [48], which may be considered more general than the FitzHugh–Nagumo model but exhibit some mathematical difficulties. We mention for instance the complexity to prove the existence and uniqueness of a weak solution. The physiological models, based on the cell membrane formulation developed by Hodgkin-Huxley [40] for nerve fibers, are more realistic and capture several physical phenomena at different scales such as the mechanical response of the medium or the microscopic behavior of chemical species. However, the mathematical models developed in this context are systems of nonlinear and parabolic PDEs coupled with multiple ODEs. Numerical simulation would involve many unknowns and an unaffordable computational cost and memory burden. We end this remark by highlighting other physiological models such as the Beeler-Reuter model [12], which was the first ventricular membrane model of mammalian cardiac myocytes; and the Luo and Rudy model [45].

2.2 Weak formulation

Before we define our discretization scheme, we start by stating the weak formulation associated with Problem (2.1). Here, we use for $r > 2$ the norm

$$\|\cdot\|_{L^2(0,T;H^1(\Omega))\cap L^r(\Omega_T)} = \max\left\{\|\cdot\|_{L^2(0,T;H^1(\Omega))}, \|\cdot\|_{L^r(\Omega_T)}\right\}$$

and the dual norm

$$\|v\|_{L^2(0,T;(H^1(\Omega))')+L^{r/(r-1)}(\Omega_T)} = \inf_{v=v_1+v_2}\left\{\|v_1\|_{L^2(0,T;(H^1(\Omega))')} + \|v_2\|_{L^{r/(r-1)}(\Omega_T)}\right\}.$$

It is easy to see that $L^2\left(0,T;(H^1(\Omega))'\right) + L^{r/(r-1)}(\Omega_T) \subset L^{r/(r-1)}\left(0,T;(H^1(\Omega))'\right)$ since $\frac{r}{r-1} \leq 2$ and $L^{r/(r-1)}(\Omega) \subset (H^1(\Omega))'$ (Sobolev inequality). Hence $\partial_t v$ remains in a bounded set of $L^{r/(r-1)}\left(0,T;(H^1(\Omega))'\right)$ while v remains in a bounded set of $L^2\left(0,T;H^1(\Omega)\right)$ (see [15]).

Definition 2.4. *Given* $f \in L^2(0,T;\left(H^1(\Omega)\right)')$, $g \in L^2(0,T;L^2(\Omega))$, $v_0 \in L^2(\Omega)$, $w_0 \in L^2(\Omega)$ *and* $\Lambda \in L^\infty(\Omega)$, *a weak solution of problem* (2.1) *is a vector* $\mathbf{U} := (v,w)$ *of functions such that* $v \in L^2\left(0,T;H^1(\Omega)\right)\cap L^r(\Omega_T)$, $r \geq 2$, $\partial_t v \in L^2\left(0,T;\left(H^1(\Omega)\right)'\right) + L^{r/(r-1)}(\Omega_T)$ *and* $w \in C(0,T;L^2(\Omega))$ *verifying*

$$\frac{d}{dt}\langle v(t),\varphi\rangle_{(H^1(\Omega))',H^1(\Omega)} + (\Lambda\boldsymbol{\nabla}v(t),\boldsymbol{\nabla}\varphi)_\Omega = -\langle f(v(t),w(t)),\varphi\rangle_{(H^1(\Omega))',H^1(\Omega)}$$

$$(\partial_t w(t),\phi)_\Omega = -(g(v(t),w(t)),\phi)_\Omega \qquad (2.4)$$

$$\forall\varphi \in H^1(\Omega),\quad \forall\phi \in L^2(\Omega).$$

Regarding the monodomain problem (2.1), the existence of its weak solution is given in the following theorem

Theorem 2.5 (Well-posedness of Monodomain Model). *Assume that the conditions listed in Assuptions 2.1, 2.2 hold. Then, the monodomain problem* (2.1) *possesses a unique weak solution in the sense of Definition 2.4. Furthermore, this solution verifies the following a priori estimates: for any* $t \in (0,T)$ *there exists constants* $\mathcal{C}_1$, $\mathcal{C}_2$, $\mathcal{C}_3$, $\mathcal{C}_4 > 0$ *such that*

$$\|v\|_{L^\infty(0,t;L^2(\Omega))} + \|w\|_{L^\infty(0,t;L^2(\Omega))} \leq \mathcal{C}_1$$

$$\|v\|_{L^2(0,t;H^1(\Omega))\cap L^r(\Omega_t)} \leq \mathcal{C}_2$$

$$\|\partial_t v\|_{L^2(0,t;L^2(\Omega))} + \|\partial_t v\|_{L^2(0,t;(H^1(\Omega))')+L^{r/(r-1)}(\Omega_t)} \leq \mathcal{C}_3$$

$$\|\partial_t w\|_{L^2(\Omega_t)} \leq \mathcal{C}_4.$$

Proof. The proof of Theorem 2.5 is standard and relies on semigroup arguments presented in [15, Lemma 31] or on the Faedo-Galerkin procedure (see [9] and the references therein). □

3 Discretization by finite elements

We now present the discretization and linearization of our model. The discretization relies on the backward Euler scheme in time and the conforming finite element method of degree $p \geq 1$ in space.

3.1 Time Discretization

For the time discretization, we introduce a division of the interval $[0,T]$ into subintervals $I_{n+1} := [t_{n-1},t_n]$, $1 \leq n \leq N_t$, such that $0 = t_0 < t_1 < \cdots < t_{N_t} = T$. The time steps are denoted by $\Delta t_n = t_n - t_{n-1}$, with $n = 1,\ldots,N_t$.

For a function of time v with sufficient regularity, we denote $v^n := v(t_n)$, $0 \leq n \leq N_t$, and, for $1 \leq n \leq N_t$, we define the backward differencing operator

$$\partial_t v^n := \frac{1}{\Delta t_n}\left(v^n - v^{n-1}\right).$$

3.2 Space Discretization

Let $\mathcal{T}_h$ be a conforming mesh of Ω, i.e. $\mathcal{T}_h$ is a set of triangles verifying

$$\bigcup_{K \in \mathcal{T}_h} \bar{K} = \bar{\Omega}$$

where the intersection of the closure of two elements of $\mathcal{T}_h$ is either an empty set, a vertex, or an edge. The set of vertices of $\mathcal{T}_h$ is denoted by $\mathcal{V}_h$ and is partitioned into the interior vertices $\mathcal{V}_h^{\text{int}}$ and the boundary vertices $\mathcal{V}_h^{\text{ext}}$. We denote by $\mathcal{N}_h^{\text{int}}$ the number of interior vertices and by $\mathcal{N}_h^{\text{ext}}$ the number of boundary vertices. Then, $\mathcal{N}_h$ denotes the total number of vertices. The vertices of an element $K \in \mathcal{T}_h$ are collected in the set $\mathcal{V}_K$. For $K \in \mathcal{T}_h$, h_K denotes the diameter of a triangle K. Then, we define the mesh diameter by $h := \max_{K \in \mathcal{T}_h} h_K$. Furthermore, for $\boldsymbol{a} \in \mathcal{V}_h$, let the patch $\omega_h^{\boldsymbol{a}} \subset \Omega$ be the domain made up of the elements of $\mathcal{T}_h$ that share $\boldsymbol{a}$. The vector $\mathbf{n}_{\omega_h^{\boldsymbol{a}}}$ represents its outward unit normal.

We use the discrete conforming space of piecewise polynomial functions

$$X_h^p := \left\{ v_h \in \mathcal{C}^0(\bar{\Omega}); \ v_h|_K \in \mathbb{P}_p(K) \ \forall K \in \mathcal{T}_h \right\} \subset H^1(\Omega)$$

where $\mathbb{P}_p(K)$ stands for the set of polynomials of total degree less than or equal to $p \geq 1$ on the element $K \in \mathcal{T}_h$. We also denote by $\mathcal{V}_d^p$ the set of the Lagrange nodes (points $\boldsymbol{x}_l$) of the space X_h^p and by $\mathcal{N}_d^p$ its cardinality. The internal Lagrange nodes are collected in the set $\mathcal{V}_{\mathrm{d}}^{p,\text{int}}$ (with $\mathcal{N}_{\mathrm{d}}^{p,\text{int}}$ its cardinality) and the external ones are collected in the set $\mathcal{V}_{\mathrm{d}}^{p,\text{ext}}$ (with $\mathcal{N}_{\mathrm{d}}^{p,\text{ext}}$ its cardinality). The Lagrange basis functions of X_h^p are denoted by $(\psi_{h,\boldsymbol{x}_l})_{1 \leq l \leq \mathcal{N}_d^p}$ for $\boldsymbol{x}_l \in \mathcal{V}_d^p$. We recall that $\psi_{h,\boldsymbol{x}_l}(\boldsymbol{x}_l) = 1$ and $\psi_{h,\boldsymbol{x}_l}(\boldsymbol{x}_{l'}) = 0$ for all $(\boldsymbol{x}_{l'})_{1 \leq l' \neq l \leq \mathcal{N}_d^p} \in \mathcal{V}_d^p$. In the particular case $p = 1$, the set $\mathcal{V}_{\mathrm{d}}^1$ coincides with the mesh vertices $\mathcal{V}_h$ and the Lagrange basis functions are the "hat" basis functions and are denoted by $\psi_{h,\boldsymbol{a}}, \boldsymbol{a} \in \mathcal{V}_h$.

Discrete problem Let $p \geq 1$. Given $(v_h^0, w_h^0) \in X_h^p \times X_h^p$, a discrete formulation corresponding to (2.4) consists in searching for all $1 \leq n \leq N_{\mathrm{t}}$, $\mathbf{U}_h^n := (v_h^n; w_h^n) \in X_h^p \times X_h^p$ such that

$$\frac{1}{\Delta t_n} \left(v_h^n - v_h^{n-1}, \varphi_h \right)_\Omega + (\Lambda \boldsymbol{\nabla} v_h^n, \boldsymbol{\nabla} \varphi_h)_\Omega = -\left(f(v_h^n, w_h^n), \varphi_h \right)_\Omega \tag{3.1a}$$

$$\frac{1}{\Delta t_n} \left(w_h^n - w_h^{n-1}, \phi_h \right)_\Omega = -\left(g(v_h^n, w_h^n), \phi_h \right)_\Omega, \tag{3.1b}$$

for all φ_h and ϕ_h in X_h^p. We want to express the discrete problem (3.1) under an algebraic form. Let $p \geq 1$ and let (v_h^n, w_h^n) be the solution of problem (3.1). First, we decompose v_h^n and w_h^n in the Lagrange basis as follows

$$v_h^n = \sum_{l=1}^{\mathcal{N}_d^p} [\boldsymbol{X}_{1h}^n]_l \, \psi_{h,\boldsymbol{x}_l}, \quad w_h^n = \sum_{l=1}^{\mathcal{N}_d^p} [\boldsymbol{X}_{2h}^n]_l \, \psi_{h,\boldsymbol{x}_l}, \tag{3.2}$$

$$\text{where} \quad \boldsymbol{X}_h^n := (\boldsymbol{X}_{1h}^n, \boldsymbol{X}_{2h}^n) \in \mathbb{R}^{2\mathcal{N}_d^p},$$

with $(\psi_{h,\boldsymbol{x}_l})_{1 \leq l \leq \mathcal{N}_d^p}$ the Lagrange basis for $p \geq 2$ and $[\boldsymbol{X}_{1h}^n]_l := v_h^n(\boldsymbol{x}_l)$ and $[\boldsymbol{X}_{2h}^n]_l := w_h^n(\boldsymbol{x}_l)$. We denote by $\mathbb{S} \in \mathbb{R}^{\mathcal{N}_d^p, \mathcal{N}_d^p}$ respectively $\mathbb{M} \in \mathbb{R}^{\mathcal{N}_d^p, \mathcal{N}_d^p}$, the stiffness matrix, respectively the mass matrix defined by

$$\mathbb{S}_{l,m} := (\Lambda \boldsymbol{\nabla} \psi_{h,\boldsymbol{x}_l}, \boldsymbol{\nabla} \psi_{h,\boldsymbol{x}_m})_\Omega, \text{ and } \mathbb{M}_{l,m} := (\psi_{h,\boldsymbol{x}_l}, \psi_{h,\boldsymbol{x}_m})_\Omega \tag{3.3}$$
$$\forall 1 \leq l, m \leq \mathcal{N}_d^p.$$

Taking $\varphi_h = \psi_{h,\boldsymbol{x}_m}$ in the first line of (3.1) and $\phi_h = \psi_{h,\boldsymbol{x}_m}$ in the second line of (3.1) for all $1 \leq m \leq \mathcal{N}_d^p$ we get

$$\frac{1}{\Delta t_n} \mathbb{M} \boldsymbol{X}_{1h}^n + \mathbb{S} \boldsymbol{X}_{1h}^n = \frac{1}{\Delta t_n} \mathbb{M} \boldsymbol{X}_{1h}^{n-1} - \boldsymbol{F}(\boldsymbol{X}_h^n)$$

$$\frac{1}{\Delta t_n} \mathbb{M} \boldsymbol{X}_{2h}^n = \frac{1}{\Delta t_n} \mathbb{M} \boldsymbol{X}_{2h}^{n-1} - \boldsymbol{G}(\boldsymbol{X}_h^n)$$

where the nonlinear function $\boldsymbol{F} : \mathbb{R}^{2\mathcal{N}_d^p} \to \mathbb{R}^{\mathcal{N}_d^p}$ is defined by

$$[\boldsymbol{F}(\boldsymbol{X})]_l = (f(v, w), \psi_{h,\boldsymbol{x}_l})_\Omega \quad \forall 1 \le l \le \mathcal{N}_d^p. \tag{3.4}$$

Here, $\boldsymbol{X} = [\boldsymbol{X}_1, \boldsymbol{X}_2]$ and v respectively w is the functional representation of $\boldsymbol{X}_1$, respectively $\boldsymbol{X}_2$. Employing Assumption 2.2 we also get

$$\begin{aligned}
[\boldsymbol{F}(\boldsymbol{X})]_l &= (f_1(v), \psi_{h,\boldsymbol{x}_l})_\Omega + (f_2(w), \psi_{h,\boldsymbol{x}_l})_\Omega \quad \forall 1 \le l \le \mathcal{N}_d^p \\
&= (f_1(v), \psi_{h,\boldsymbol{x}_l})_\Omega + (\lambda w, \psi_{h,\boldsymbol{x}_l})_\Omega \quad \forall 1 \le l \le \mathcal{N}_d^p.
\end{aligned} \tag{3.5}$$

Matricially (3.5) reads as

$$\boldsymbol{F}(\boldsymbol{X}) := \tilde{\boldsymbol{F}}(\boldsymbol{X}_1) + \lambda \mathbb{M} \boldsymbol{X}_2 \tag{3.6}$$

where $\left[\tilde{\boldsymbol{F}}(\boldsymbol{X}_1)\right]_l := (f_1(v), \psi_{h,\boldsymbol{x}_l})_\Omega \ \forall 1 \le l \le \mathcal{N}_d^p$. Furthermore, the function $\boldsymbol{G} : \mathbb{R}^{2\mathcal{N}_d^p} \to \mathcal{N}_d^p$ is defined by

$$[\boldsymbol{G}(\boldsymbol{X})]_l := (g(v, w), \psi_{h,\boldsymbol{x}_l})_\Omega \quad \forall 1 \le l \le \mathcal{N}_d^p.$$

Furthermore, as the function g is linear, we have

$$\boldsymbol{G}(\boldsymbol{X}_h^n) = -a\mathbb{M}\boldsymbol{X}_{1h}^n + b\mathbb{M}\boldsymbol{X}_{2h}^n. \tag{3.7}$$

Observe that the first term in (3.5) is nonlinear since the function f_1 is intrinsically nonlinear. We could not express it conveniently as in (3.7). This term will be treated afterward thanks to a linearization Newton scheme. Finally, we obtain the compact nonlinear system of algebraic equations: given $\boldsymbol{X}_h^{n-1} \in \mathbb{R}^{2\mathcal{N}_d^p}$ find $\boldsymbol{X}_h^n \in \mathbb{R}^{2\mathcal{N}_d^p}$ solution to

$$\begin{cases} \mathcal{S}_1(\boldsymbol{X}_h^n) = 0 \\ \mathcal{S}_2(\boldsymbol{X}_h^n) = 0 \end{cases} \tag{3.8}$$

where $\mathcal{S}_1 : \mathbb{R}^{2\mathcal{N}_d^p} \to \mathbb{R}^{\mathcal{N}_d^p}$ and $\mathcal{S}_2 : \mathbb{R}^{2\mathcal{N}_d^p} \to \mathbb{R}^{\mathcal{N}_d^p}$ are defined locally by

$$\begin{aligned}
[\mathcal{S}_1(\boldsymbol{X}_h^n)]_l &= \frac{1}{\Delta t_n}[\mathbb{M}\boldsymbol{X}_{1h}^n]_l + [\mathbb{S}\boldsymbol{X}_{1h}^n]_l + [\boldsymbol{F}(\boldsymbol{X}_h^n)]_l - \frac{1}{\Delta t_n}[\mathbb{M}\boldsymbol{X}_{1h}^{n-1}]_l \\
[\mathcal{S}_2(\boldsymbol{X}_h^n)]_l &= \frac{1}{\Delta t_n}[\mathbb{M}\boldsymbol{X}_{2h}^n]_l - a[\mathbb{M}\boldsymbol{X}_{1h}^n]_l + b[\mathbb{M}\boldsymbol{X}_{2h}^n]_l - \frac{1}{\Delta t_n}[\mathbb{M}\boldsymbol{X}_{2h}^{n-1}]_l
\end{aligned} \tag{3.9}$$

for $l \in [\![1, \mathcal{N}_d^p]\!]$.

Introducing the operator $\mathcal{S} : \mathbb{R}^{2\mathcal{N}_d^p} \to \mathbb{R}^{2\mathcal{N}_d^p}$ such that

$$\mathcal{S}(\boldsymbol{X}) := [\mathcal{S}_1(\boldsymbol{X}), \mathcal{S}_2(\boldsymbol{X})] \tag{3.10}$$

we have to solve the equation $\mathcal{S}(\boldsymbol{X}_h^n) = 0$. We present in the sequel at each time step $1 \le n \le N_t$ a Newton algorithm to approximate the solution of system (3.10).

3.3 Newton method

Let $p \ge 1$ be given. The Newton algorithm is defined as follows. For $1 \le n \le N_t$ and $\boldsymbol{X}_h^{n,0} \in \mathbb{R}^{2\mathcal{N}_d^p}$ fixed, typically, $\boldsymbol{X}_h^{n,0} := \boldsymbol{X}_h^{n-1}$ where $\boldsymbol{X}_h^{n-1}$ is the last iterate from the previous time step, one looks at step $k \ge 1$ for $\boldsymbol{X}_h^{n,k} \in \mathbb{R}^{2\mathcal{N}_d^p}$ such that

$$\mathbb{A}^{n,k-1}\boldsymbol{X}_h^{n,k} = \boldsymbol{B}^{n,k-1}. \tag{3.11}$$

Here, the Jacobian matrix $\mathbb{A}^{n,k-1} \in \mathbb{R}^{2\mathcal{N}_d^p, 2\mathcal{N}_d^p}$ and the right hand side vector $\boldsymbol{B}^{n,k-1} \in \mathbb{R}^{2\mathcal{N}_d^p}$ are defined by

$$\mathbb{A}^{n,k-1} := \mathbb{J}_\mathcal{S}(\boldsymbol{X}_h^{n,k-1}) \text{ and } \boldsymbol{B}^{n,k-1} := \mathbb{J}_\mathcal{S}(\boldsymbol{X}_h^{n,k-1})\boldsymbol{X}_h^{n,k-1} - \mathcal{S}(\boldsymbol{X}_h^{n,k-1}) \tag{3.12}$$

where $\mathbb{J}_\mathcal{S}(\boldsymbol{X}_h^{n,k-1})$ is the Jacobian matrix of the function $\mathcal{S}$ at point $\boldsymbol{X}_h^{n,k-1}$ obtained by a Newton linearization. More precisely,

$$\mathbb{A}^{n,k-1} := \begin{pmatrix} \frac{1}{\Delta t_n}\mathbb{M} + \mathbb{S} + \mathbb{J}_{\tilde{\boldsymbol{F}}}(\boldsymbol{X}_{1h}^{n,k-1}) & \lambda\mathbb{M} \\ -a\mathbb{M} & \left(b + \frac{1}{\Delta t_n}\right)\mathbb{M} \end{pmatrix}$$

7

and

$$\boldsymbol{B}^{n,k-1} := \begin{pmatrix} \mathbb{J}_{\tilde{\boldsymbol{F}}}(\boldsymbol{X}_{1h}^{n,k-1}) & \lambda\mathbb{M} \\ 0\mathbb{I}_{\mathcal{N}_d^p,\mathcal{N}_d^p} & 0\mathbb{I}_{\mathcal{N}_d^p,\mathcal{N}_d^p} \end{pmatrix} \boldsymbol{X}_h^{n,k-1} + \begin{pmatrix} \frac{1}{\Delta t_n}\mathbb{M} & 0\mathbb{I}_{\mathcal{N}_d^p,\mathcal{N}_d^p} \\ 0\mathbb{I}_{\mathcal{N}_d^p,\mathcal{N}_d^p} & \frac{1}{\Delta t_n}\mathbb{M} \end{pmatrix} \boldsymbol{X}_h^{n-1}$$
$$- \begin{pmatrix} \boldsymbol{F}(\boldsymbol{X}_h^{n,k-1}) \\ \boldsymbol{0} \end{pmatrix}.$$

Here, the Jacobian matrix of the vectorial function $\tilde{\boldsymbol{F}}$ is defined by

$$\left[\mathbb{J}_{\tilde{\boldsymbol{F}}}(\boldsymbol{X}_{1h}^{n,k-1}) \right]_{l,m} := \left(f_1'(v_h^{n,k-1})\psi_{h,\boldsymbol{x}_m}, \psi_{h,\boldsymbol{x}_l} \right)_\Omega \quad \forall 1 \le l,m \le \mathcal{N}_d^p.$$

In the exact Newton method, the linear system (3.11) is solved exactly. For the linearization stopping criterion, we choose a tolerance ε close to the machine precision and stop the linearization procedure when the error satisfies

$$\left\| \boldsymbol{X}_h^{n,k} - \boldsymbol{X}_h^{n-1} \right\|_\infty \le \varepsilon. \tag{3.13}$$

Remark 3.1. *The numerical computation of $\tilde{\boldsymbol{F}}(\boldsymbol{X}_{1h}^{n,k-1})$ as well as $\mathbb{J}_{\tilde{\boldsymbol{F}}}(\boldsymbol{X}_{1h}^{n,k-1})$ is tricky. Indeed, their computation requires the knowledge of the function $v_{1h}^{n,k-1}$, which is not suitable. To tackle this difficulty, two main approaches are presented in the literature: Ionic Current Interpolation (ICI) and State Variable Interpolation (SVI). The ICI method is widely adopted in the cardiac modeling community, as noted by Gray et al. [50] and Pezzuto et al. [51]. This approach relies on interpolating the ionic current after its evaluation at the Lagrange nodes.*
Alternatively, the SVI method first interpolates individual state variables, such as the transmembrane potential v and the gate variable w at the quadrature nodes before evaluating the ionic current function f at these interpolated points. Although SVI can potentially offer higher accuracy in some scenarios, it induces a significant computational cost, especially for complex ionic models with numerous state variables, as highlighted by Pezzuto et al. [59].
In this work, we employed the ICI methodology. Therefrom, the nonlinear term $f_1(v_h)$ computed as follows :

$$f_1(v_h) = \sum_{l=1}^{\mathcal{N}_d^p} f_1\left([\boldsymbol{X}_{1h}]_l\right) \psi_{h,\boldsymbol{x}_l}.$$

Hence, we can express the nonlinear term $\tilde{\boldsymbol{F}}$ in (3.6) and its corresponding Jacobian matrix by

$$\tilde{\boldsymbol{F}}(\boldsymbol{X}_{1h}^{n,k-1}) = \mathbb{M}\hat{\boldsymbol{F}}(\boldsymbol{X}_{1h}^{n,k-1}) \text{ and } \quad \mathbb{J}_{\tilde{\boldsymbol{F}}}(\boldsymbol{X}_{1h}^{n,k-1}) = \mathbb{M}\mathbb{D}^T$$

where the vector $\hat{\boldsymbol{F}} \in \mathbb{R}^{\mathcal{N}_d^p}$ and the diagonal matrix $\mathbb{D} \in \mathbb{R}^{\mathcal{N}_d^p, \mathcal{N}_d^p}$ are defined by

$$\left[\hat{\boldsymbol{F}}(\boldsymbol{X}_{1h}^{n,k-1})\right]_l := f_1\left(\left[\boldsymbol{X}_{1h}^{n,k-1}\right]_l\right) \text{ and } \quad \mathbb{D}_{l,l} := f_1'\left(\left[\boldsymbol{X}_{1h}^{n,k-1}\right]_l\right) \quad \forall 1 \le l \le \mathcal{N}_d^p.$$

4 A posteriori error analysis

4.1 Preamble

At each time step $1 \le n \le N_{\mathrm{t}}$, we have presented the nonlinear system (3.8) giving, in particular, the degrees of freedom of the linearized numerical solution $\boldsymbol{X}_h^{n,k} \in \mathbb{R}^{2\mathcal{N}_d^p}$. The functional representation of the vectors $\boldsymbol{X}_{1h}^{n,k}$ and $\boldsymbol{X}_{2h}^{n,k}$, denoted by $v_h^{n,k}$ and $w_h^{n,k}$ are given by (3.2) for $p \ge 1$. Obviously, $\left(v_h^{n,k}, w_h^{n,k}\right) \in X_h^p \times X_h^p \quad \forall 1 \le n \le N_{\mathrm{t}}$. Next, we associate to the functions in space $v_h^{n,k} \in X_h^p$, and $w_h^{n,k} \in X_h^p$, $1 \le n \le N_{\mathrm{t}}$, their space-time representation $v_{h\tau}^k$, respectively $w_{h\tau}^k$ as follows:

$$\begin{aligned} v_{h\tau}^k|_{I_n} &:= \frac{v_h^{n,k} - v_h^{n-1}}{\Delta t_n}(t - t^n) + v_h^{n,k} \quad \forall 1 \le n \le N_{\mathrm{t}}, \\ w_{h\tau}^k|_{I_n} &:= \frac{w_h^{n,k} - w_h^{n-1}}{\Delta t_n}(t - t^n) + w_h^{n,k} \quad \forall 1 \le n \le N_{\mathrm{t}}. \end{aligned} \tag{4.1}$$

Note that this construction ensures that $v_{h\tau}^k$ and $w_{h\tau}^k$ are piecewise affine and continuous in time, so that $\partial_t v_{h\tau}^k \in L^2\left(0, T; \left(H^1(\Omega)\right)'\right) + L^{r/(r-1)}(\Omega_T)$ and $\partial_t w_{h\tau}^k \in L^2\left(0, T; L^2(\Omega)\right)$. In the expressions of $v_{h\tau}^k$ and $w_{h\tau}^k$, the index k is kept to indicate the presence of a nonlinear solver. For each unknown, we note

$$v_{h\tau}^{n,k} := v_{h\tau}^k\big|_{I_n}, \quad w_{h\tau}^{n,k} := w_{h\tau}^k\big|_{I_n}.$$

Note that consequently

$$\partial_t v_{h\tau}^{n,k}\Big|_{I_n} = \frac{1}{\Delta t_n}\left(v_h^{n,k} - v_h^{n-1}\right), \quad \partial_t w_{h\tau}^{n,k}\Big|_{I_n} = \frac{1}{\Delta t_n}\left(w_h^{n,k} - w_h^{n-1}\right).$$

Our a posteriori analysis relies on the equilibrated flux reconstructions following the concept of Destuynder and Métivet [26], Braess and Schöberl [16], Dabaghi *et al.* [24, 25], Ern and Vohralík [31]. Since the reaction-diffusion equation in (2.1) is nonlinear we need to build two equilibrated flux reconstruction $\left(\boldsymbol{\sigma}_{h,\mathrm{disc}}^{n,k}, \boldsymbol{\sigma}_{h,\mathrm{lin}}^{n,k}\right) \in [\mathbf{H}(\mathrm{div}, \Omega)]^2$ to recover fully the structural properties violated by the approximate solution. More precisely, these fluxes are obtained by solving mixed finite element systems on the patches $\omega_h^{\boldsymbol{a}}$ around the mesh vertices $\boldsymbol{a} \in \mathcal{V}_h$ on the mesh $\mathcal{T}_h$. It is easily seen that the first equation of Problem (3.11) reads

$$\begin{aligned}
&\frac{1}{\Delta t_n}\left(v_h^{n,k} - v_h^{n-1}, \psi_{h,\boldsymbol{x}_l}\right)_\Omega + \left(\Lambda \boldsymbol{\nabla} v_h^{n,k}, \boldsymbol{\nabla}\psi_{h,\boldsymbol{x}_l}\right)_\Omega \\
&+ \left(\mathcal{F}^{n,k}(v_h^{n,k}, w_h^{n,k}), \psi_{h,\boldsymbol{x}_l}\right)_\Omega = 0
\end{aligned} \tag{4.2}$$

where

$$\begin{aligned}
\mathcal{F}^{n,k}(v_h^{n,k}, w_h^{n,k}) &:= f_1'(v_h^{n,k-1})\left(v_h^{n,k} - v_h^{n,k-1}\right) + f_2'(w_h^{n,k-1})\left(w_h^{n,k} - w_h^{n,k-1}\right) \\
&+ f(v_h^{n,k-1}, w_h^{n,k-1}).
\end{aligned}$$

The functional representation of (3.11) given by (4.2) is essential for our a posteriori analysis as we will see in the sequel. The fluxes $\boldsymbol{\sigma}_{h,\mathrm{disc}}^{n,k}$ and $\boldsymbol{\sigma}_{h,\mathrm{lin}}^{n,k}$ are reconstructed in the Raviart-Thomas subspaces of $\mathbf{H}(\mathrm{div}, \Omega)$. We recall that the Raviart-Thomas spaces of order $p \geq 1$ are defined by

$$\mathbf{RT}_p(\Omega) := \left\{\boldsymbol{\tau}_h \in \mathbf{H}(\mathrm{div}, \Omega), \boldsymbol{\tau}_h|_K \in \mathbf{RT}_p(K) \quad \forall K \in \mathcal{T}_h\right\},$$

where $\mathbf{RT}_p(K) := [\mathbb{P}_p(K)]^2 + \overrightarrow{\boldsymbol{x}}\mathbb{P}_p(K)$, with $\overrightarrow{\boldsymbol{x}} = [x_1, x_2]^T$. For $\boldsymbol{a} \in \mathcal{V}_h$, let

$$\mathbf{RT}_p(\omega_h^{\boldsymbol{a}}) := \left\{\boldsymbol{\tau}_h \in \mathbf{H}(\mathrm{div}, \omega_h^{\boldsymbol{a}}), \boldsymbol{\tau}_h|_K \in \mathbf{RT}_p(K), \forall K \in \mathcal{T}_h \text{ such that } K \subset \omega_h^{\boldsymbol{a}}\right\},$$

be the restriction of the Raviart–Thomas space to the patch $\omega_h^{\boldsymbol{a}}$, and let $\mathbb{P}_p\left(\mathcal{T}_h|_{\omega_h^{\boldsymbol{a}}}\right)$ stand for piecewise discontinuous polynomials of order p in the patch $\omega_h^{\boldsymbol{a}}$. Define consequently the spaces $\mathbf{V}_h^{\boldsymbol{a}}$ and $Q_h^{\boldsymbol{a}}$, when $\boldsymbol{a} \in \mathcal{V}_h^{\mathrm{int}}$ by

$$\mathbf{V}_h^{\boldsymbol{a}} := \left\{\boldsymbol{\tau}_h \in \mathbf{RT}_p(\omega_h^{\boldsymbol{a}}), \boldsymbol{\tau}_h \cdot \mathbf{n}_{\omega_h^{\boldsymbol{a}}} = 0 \text{ on } \partial\omega_h^{\boldsymbol{a}}\right\}, \tag{4.3}$$

$$Q_h^{\boldsymbol{a}} := \left\{q_h \in \mathbb{P}_p\left(\mathcal{T}_h|_{\omega_h^{\boldsymbol{a}}}\right), (q_h, 1)_{\omega_h^{\boldsymbol{a}}} = 0\right\},$$

and when $\boldsymbol{a} \in \mathcal{V}_h^{\mathrm{ext}}$ by

$$\mathbf{V}_h^{\boldsymbol{a}} := \left\{\boldsymbol{\tau}_h \in \mathbf{RT}_p(\omega_h^{\boldsymbol{a}}), \boldsymbol{\tau}_h \cdot \mathbf{n}_{\omega_h^{\boldsymbol{a}}} = 0 \text{ on } \partial\omega_h^{\boldsymbol{a}} \backslash \partial\Omega\right\}, Q_h^{\boldsymbol{a}} := \mathbb{P}_p\left(\mathcal{T}_h|_{\omega_h^{\boldsymbol{a}}}\right). \tag{4.4}$$

Remark 4.1. *Observe from the construction of the discrete spaces in (4.3) and (4.4) that if $\boldsymbol{\theta}_h \in \mathbf{V}_h^{\boldsymbol{a}}$ then $\boldsymbol{\theta}_h \in \boldsymbol{H}(\mathrm{div}, \Omega)$. In Section 4.2, we develop the construction of the total flux $\boldsymbol{\sigma}_{h,\mathrm{tot}}^{n,k}$ defined as the sum of the discretization flux $\boldsymbol{\sigma}_{h,\mathrm{disc}}^{n,k}$ and the linearization flux $\boldsymbol{\sigma}_{h,\mathrm{lin}}^{n,k}$. Next, we propose the construction of the discretization flux $\boldsymbol{\sigma}_{h,\mathrm{disc}}^{n,k}$. Therefrom, we immediately obtain the linearization flux.*

4.2 Total flux reconstruction

For all time steps $1 \leq n \leq N_{\mathrm{t}}$, and all Newton step $k \geq 1$, let $\left(v_h^{n,k}, w_h^{n,k} \right)$ be the approximate solution given by (3.11), verifying in particular (4.2). For each vertex $\boldsymbol{a} \in \mathcal{V}_h$, define $\boldsymbol{\sigma}_{h,\mathrm{tot}}^{n,k,\boldsymbol{a}} \in \mathbf{V}_h^{\boldsymbol{a}}$ and $\gamma_h^{n,\boldsymbol{a}} \in Q_h^{\boldsymbol{a}}$, by solving:

$$
\begin{aligned}
\left(\boldsymbol{\sigma}_{h,\mathrm{tot}}^{n,k,\boldsymbol{a}}, \boldsymbol{\tau}_h \right)_{\omega_h^{\boldsymbol{a}}} - \left(\gamma_h^{n,k,\boldsymbol{a}}, \boldsymbol{\nabla} \cdot \boldsymbol{\tau}_h \right)_{\omega_h^{\boldsymbol{a}}} &= - \left(\psi_{h,\boldsymbol{a}} \Lambda \boldsymbol{\nabla} v_h^{n,k}, \boldsymbol{\tau}_h \right)_{\omega_h^{\boldsymbol{a}}} && \forall \boldsymbol{\tau}_h \in \mathbf{V}_h^{\boldsymbol{a}}, \\
\left(\boldsymbol{\nabla} \cdot \boldsymbol{\sigma}_{h,\mathrm{tot}}^{n,k,\boldsymbol{a}}, q_h \right)_{\omega_h^{\boldsymbol{a}}} &= \left(\hat{f}_h^{n,k,\boldsymbol{a}}, q_h \right)_{\omega_h^{\boldsymbol{a}}} && \forall q_h \in Q_h^{\boldsymbol{a}},
\end{aligned}
\tag{4.5}
$$

where the spaces $\mathbf{V}_h^{\boldsymbol{a}}$ and $Q_h^{\boldsymbol{a}}$ are defined by (4.3)-(4.4). The right-hand side function $\hat{f}_h^{n,k,\boldsymbol{a}}$ is defined by

$$
\hat{f}_h^{n,k,\boldsymbol{a}} := \frac{1}{\Delta t_n} \left(v_h^{n,k} - v_h^{n-1} \right) \psi_{h,\boldsymbol{a}} + \Lambda \boldsymbol{\nabla} v_h^{n,k} \cdot \boldsymbol{\nabla} \psi_{h,\boldsymbol{a}} + \mathcal{F}^{n,k}(v_h^{n,k}, w_h^{n,k}) \psi_{h,\boldsymbol{a}}
$$

As a result of (4.2) we note that

$$
\left(\hat{f}_h^{n,k,\boldsymbol{a}}, 1 \right)_{\omega_h^{\boldsymbol{a}}} = 0.
\tag{4.6}
$$

This implies the Neumann compatibility condition for (4.5). At each time step $1 \leq n \leq N_{\mathrm{t}}$ the total flux reconstruction is defined by

$$
\boldsymbol{\sigma}_{h,\mathrm{tot}}^{n,k} = \sum_{\boldsymbol{a} \in \mathcal{V}_h} \boldsymbol{\sigma}_{h,\mathrm{tot}}^{n,k,\boldsymbol{a}}.
$$

Proposition 4.2. *The total flux reconstruction $\boldsymbol{\sigma}_{h,\mathrm{tot}}^{n,k} \in \boldsymbol{H}(\mathrm{div}, \Omega)$ and satisfies the equilibration property* $\forall K \in \mathcal{T}_h$

$$
\left(\boldsymbol{\nabla} \cdot \boldsymbol{\sigma}_{h,\mathrm{tot}}^{n,k}, q_h \right)_K = \left(\mathcal{F}^{n,k}(v_h^{n,k}, w_h^{n,k}) + \partial_t v_{h\tau}^{n,k}, q_h \right)_K \quad \forall q_h \in \mathbb{P}_p(K).
\tag{4.7}
$$

Proof. First, we have $\boldsymbol{\sigma}_{h,\mathrm{tot}}^{n,k,\boldsymbol{a}} \in \boldsymbol{H}(\mathrm{div}, \omega_h^{\boldsymbol{a}})$. From Remark 4.1 we obtain that $\boldsymbol{\sigma}_{h,\mathrm{tot}}^{n,k,\boldsymbol{a}} \in \boldsymbol{H}(\mathrm{div}, \Omega)$ and thus $\boldsymbol{\sigma}_{h,\mathrm{tot}}^{n,k} \in \boldsymbol{H}(\mathrm{div}, \Omega)$. Next, for $\boldsymbol{a} \in \mathcal{V}_h^{\mathrm{int}}$, defining $\widetilde{Q}_h^{\boldsymbol{a}} := \mathbb{P}_p \left(\mathcal{T}_h|_{\omega_h^{\boldsymbol{a}}} \right)$ we have obviously the inclusion $Q_h^{\boldsymbol{a}} \subset \widetilde{Q}_h^a$ and the decomposition $q_h = q_h^* + c^*$ where $q_h \in \widetilde{Q}_h^{\boldsymbol{a}}$, $q_h^* \in Q_h^{\boldsymbol{a}}$, and $c^* = \frac{1}{|\omega_h^{\boldsymbol{a}}|} (q_h, 1)_{\omega_h^{\boldsymbol{a}}}$ a constant. Note that the spaces $\mathbf{V}_h^{\boldsymbol{a}}$ defined by (4.3)-(4.4) in combination with the Green formula gives $\left(\boldsymbol{\nabla} \cdot \boldsymbol{\sigma}_{h,\mathrm{tot}}^{n,k,\boldsymbol{a}}, 1 \right)_{\omega_h^{\boldsymbol{a}}} = \left(\boldsymbol{\sigma}_{h,\mathrm{tot}}^{n,k,\boldsymbol{a}} \cdot \boldsymbol{n}_{\omega_h^{\boldsymbol{a}}}, 1 \right)_{\partial \omega_h^{\boldsymbol{a}}} = 0$. Thus,

$$
\begin{aligned}
\left(\boldsymbol{\nabla} \cdot \boldsymbol{\sigma}_{h,\mathrm{tot}}^{n,k,\boldsymbol{a}}, q_h \right)_{\omega_h^{\boldsymbol{a}}} &= \left(\boldsymbol{\nabla} \cdot \boldsymbol{\sigma}_{h,\mathrm{tot}}^{n,k,\boldsymbol{a}}, q_h^* + c^* \right)_{\omega_h^{\boldsymbol{a}}} \\
&= \left(\boldsymbol{\nabla} \cdot \boldsymbol{\sigma}_{h,\mathrm{tot}}^{n,k,\boldsymbol{a}}, q_h^* \right)_{\omega_h^{\boldsymbol{a}}} + c^* \left(\boldsymbol{\nabla} \cdot \boldsymbol{\sigma}_{h,\mathrm{tot}}^{n,k,\boldsymbol{a}}, 1 \right)_{\omega_h^{\boldsymbol{a}}} \\
&= \left(\boldsymbol{\nabla} \cdot \boldsymbol{\sigma}_{h,\mathrm{tot}}^{n,k,\boldsymbol{a}}, q_h^* \right)_{\omega_h^{\boldsymbol{a}}} = \left(\hat{f}_h^{n,k,\boldsymbol{a}}, q_h^* \right)_{\omega_h^{\boldsymbol{a}}}.
\end{aligned}
\tag{4.8}
$$

Employing the Neumann compatibility property (4.6) we get

$$
\left(\hat{f}_h^{n,k,\boldsymbol{a}}, q_h^* \right)_{\omega_h^{\boldsymbol{a}}} = \left(\hat{f}_h^{n,k,\boldsymbol{a}}, q_h - c^* \right)_{\omega_h^{\boldsymbol{a}}} = \left(\hat{f}_h^{n,k,\boldsymbol{a}}, q_h \right)_{\omega_h^{\boldsymbol{a}}}.
$$

Finally,

$$
\left(\boldsymbol{\nabla} \cdot \boldsymbol{\sigma}_{h,\mathrm{tot}}^{n,k,\boldsymbol{a}}, q_h \right)_{\omega_h^{\boldsymbol{a}}} = \left(\hat{f}_h^{n,k,\boldsymbol{a}}, q_h \right)_{\omega_h^{\boldsymbol{a}}} \quad \forall q_h \in \widetilde{Q}_h^a.
\tag{4.9}
$$

We thus observe that the condition (4.9) holds for all piecewise polynomials belonging to $\mathbb{P}_p \left(\mathcal{T}_h|_{\omega_h^{\boldsymbol{a}}} \right)$ and not only for those with zero mean value. Next, crucial argument is that the polynomials in $\mathbb{P}_p \left(\mathcal{T}_h|_{\omega_h^{\boldsymbol{a}}} \right)$ are

discontinuous, so that we can restrict q_h to any element $K \in \mathcal{T}_h$. If $\boldsymbol{a} \in \mathcal{V}_h^{\text{ext}}$, this is immediate. Then, for any $q_h \in \mathbb{P}_p(K)$ we get

$$
\begin{aligned}
\left(\boldsymbol{\nabla} \cdot \boldsymbol{\sigma}_{h,\text{tot}}^{n,k}, q_h\right)_K &= \sum_{\boldsymbol{a} \in \mathcal{V}_K} \left(\boldsymbol{\nabla} \cdot \boldsymbol{\sigma}_{h,\text{tot}}^{n,k,\boldsymbol{a}}, q_h\right)_K = \sum_{\boldsymbol{a} \in \mathcal{V}_K} \left(\hat{f}_h^{n,k,\boldsymbol{a}}, q_h\right)_K \\
&= \sum_{\boldsymbol{a} \in \mathcal{V}_K} \left(\mathcal{F}^{n,k}(v_h^{n,k}, w_h^{n,k})\psi_{h,\boldsymbol{a}} + \partial_t v_{h\tau}^{n,k}\psi_{h,\boldsymbol{a}} + \Lambda\boldsymbol{\nabla} v_h^{n,k} \cdot \boldsymbol{\nabla}\psi_{h,\boldsymbol{a}}, q_h\right)_K .
\end{aligned}
$$

Remarking that $\sum_{a \in \mathcal{V}_K} \psi_{h,\boldsymbol{a}}\big|_K = 1$, so we get the desired property 4.2. $\qquad\square$

4.3 Discretization flux reconstruction

For all time steps $1 \le n \le N_t$, and all Newton step $k \ge 1$, let $\left(v_h^{n,k}, w_h^{n,k}\right)$ be the approximate solution given by (3.11), verifying in particular (4.2). We define for each internal vertex $\boldsymbol{a} \in \mathcal{V}_h^{\text{int}}$ the following quantity

$$
\begin{aligned}
R_{\boldsymbol{a}}^k := &\frac{1}{\Delta t_n}\left(v_h^{n,k} - v_h^{n-1}, \psi_{h,\boldsymbol{a}}\right)_{\omega_h^{\boldsymbol{a}}} + \left(\Lambda\boldsymbol{\nabla} v_h^{n,k}, \boldsymbol{\nabla}\psi_{h,\boldsymbol{a}}\right)_{\omega_h^{\boldsymbol{a}}} \\
&+ \left(f(v_h^{n,k-1}, w_h^{n,k-1}), \psi_{h,\boldsymbol{a}}\right)_{\omega_h^{\boldsymbol{a}}} .
\end{aligned}
$$

For each vertex $\boldsymbol{a} \in \mathcal{V}_h$, define $\boldsymbol{\sigma}_{h,\text{disc}}^{n,k,\boldsymbol{a}} \in \mathbf{V}_h^{\boldsymbol{a}}$ and $\gamma_h^{n,\boldsymbol{a}} \in Q_h^{\boldsymbol{a}}$, by solving:

$$
\begin{cases}
\left(\boldsymbol{\sigma}_{h,\text{disc}}^{n,k,\boldsymbol{a}}, \boldsymbol{\tau}_h\right)_{\omega_h^{\boldsymbol{a}}} - \left(\gamma_h^{n,k,\boldsymbol{a}}, \boldsymbol{\nabla} \cdot \boldsymbol{\tau}_h\right)_{\omega_h^{\boldsymbol{a}}} = -\left(\psi_{h,\boldsymbol{a}}\Lambda\boldsymbol{\nabla} v_h^{n,k}, \boldsymbol{\tau}_h\right)_{\omega_h^{\boldsymbol{a}}} & \forall \boldsymbol{\tau}_h \in \mathbf{V}_h^{\boldsymbol{a}}, \\
\left(\boldsymbol{\nabla} \cdot \boldsymbol{\sigma}_{h,\text{disc}}^{n,k,\boldsymbol{a}}, q_h\right)_{\omega_h^{\boldsymbol{a}}} = \left(\tilde{f}_h^{n,k,\boldsymbol{a}}, q_h\right)_{\omega_h^{\boldsymbol{a}}} & \forall q_h \in Q_h^{\boldsymbol{a}},
\end{cases} \quad (4.10)
$$

where the spaces $\mathbf{V}_h^{\boldsymbol{a}}$ and $Q_h^{\boldsymbol{a}}$ are defined by (4.3)-(4.4). The right-hand sides are defined by

$$
\begin{aligned}
\tilde{f}_h^{n,k,\boldsymbol{a}} := &\frac{1}{\Delta t_n}\left(v_h^{n,k} - v_h^{n-1}\right)\psi_{h,\boldsymbol{a}} + \Lambda\boldsymbol{\nabla} v_h^{n,k} \cdot \boldsymbol{\nabla}\psi_{h,\boldsymbol{a}} + f(v_h^{n,k-1}, w_h^{n,k-1})\psi_{h,\boldsymbol{a}} \\
&- \frac{1}{|\omega_h^{\boldsymbol{a}}|}R_{\boldsymbol{a}}^k .
\end{aligned}
$$

Observe that the Neumann compatibility condition is satisfied for system (4.10). At each time step $1 \le n \le N_t$ the discretization flux reconstruction is defined by

$$
\boldsymbol{\sigma}_{h,\text{disc}}^{n,k} = \sum_{\boldsymbol{a} \in \mathcal{V}_h} \boldsymbol{\sigma}_{h,\text{disc}}^{n,k,\boldsymbol{a}} .
$$

Following the methodology of Section 4.2 we get the following equilibration property.

Proposition 4.3. *The discretization flux reconstruction $\boldsymbol{\sigma}_{h,\text{disc}}^{n,k} \in \boldsymbol{H}(\text{div}, \Omega)$ and satisfies $\forall K \in \mathcal{T}_h$*

$$
\left(\boldsymbol{\nabla} \cdot \boldsymbol{\sigma}_{h,\text{disc}}^{n,k}, q_h\right)_K = \left(\partial_t v_{h\tau}^{n,k} + f(v_h^{n,k-1}, w_h^{n,k-1}) - \sum_{\boldsymbol{a} \in \mathcal{V}_K} \frac{1}{|\omega_h^{\boldsymbol{a}}|}R_{\boldsymbol{a}}^k, q_h\right)_K \quad (4.11)
$$

for all $q_h \in \mathbb{P}_p(K)$.

Proof. The proof is similar to the one presented in Proposition 4.2. $\qquad\square$

Remark 4.4. *Having constructed the total flux reconstruction $\boldsymbol{\sigma}_{h,\text{tot}}^{n,k}$ and the discretization flux reconstruction $\boldsymbol{\sigma}_{h,\text{disc}}^{n,k}$ we deduce the linearization flux reconstruction $\boldsymbol{\sigma}_{h,\text{lin}}^{n,k} = \boldsymbol{\sigma}_{h,\text{tot}}^{n,k} - \boldsymbol{\sigma}_{h,\text{disc}}^{n,k}$. Furthermore, when the Newton solver has converged, i.e. when $k \to +\infty$, the nonlinear term $\mathcal{F}^{n,k}(v_h^{n,k}, w_h^{n,k})$ coincides with $f(v_h^n, w_h^n)$ so that the equilibrium relation of Proposition 4.2 reads*

$$
\left(\boldsymbol{\nabla} \cdot \boldsymbol{\sigma}_{h,\text{tot}}^n, q_h\right)_K = (f(v_h^n, w_h^n) + \partial_t v_{h\tau}^n, q_h)_K \quad \forall q_h \in \mathbb{P}_p(K).
$$

The same phenomenon occurs for the equilibrium property given by Proposition 4.3. In this scenario (4.7) and (4.11) are identical assessing the coherence of our approach.

4.4 Residual of the equations

We denote by X_n the restriction of the energy space $X := L^2(0, T; H^1(\Omega))$ to the time interval I_n, i.e. $X_n := L^2(I_n, H^1(\Omega))$. We also denote by Y_n the restriction of the energy space $Y := L^2(0, T; L^2(\Omega))$ to the time interval I_n, i.e. $Y_n := L^2(I_n, L^2(\Omega))$. Then, we can introduce the following Sobolev space

$$Z_n := \left\{ v \in X_n; \ \partial_t v \in X_n' := L^2\left(I_n, (H^1(\Omega))'\right) \right\}$$

which is the restriction of the energy space

$$Z := \left\{ v \in X; \ \partial_t v \in X' := L^2\left(0, T; (H^1(\Omega))'\right) \right\}$$

to the time interval I_n.

For $v \in X$ the space-time energy norm on X is given by

$$\|v\|_X := \left\{ \int_0^T \|v\|_\Omega^2 (t) \, \mathrm{dt} + \int_0^T \left\| \Lambda^{\frac{1}{2}} \boldsymbol{\nabla} v \right\|_\Omega^2 (t) \, \mathrm{dt} \right\}^{\frac{1}{2}}.$$

We augment the energy norm by the dual norm of the time derivative, forming a norm on the space Z. For $v \in Z$ we set

$$\|v\|_Z := \|v\|_X + \|\partial_t v\|_{X'}$$

where

$$\|\partial_t v\|_{X'} = \left\{ \int_0^T \|\partial_t v\|_{(H^1(\Omega))'}^2 (t) \, \mathrm{dt} \right\}^{\frac{1}{2}}.$$

Here we recall that

$$\|\partial_t v\|_{(H^1(\Omega))'} := \sup_{\varphi \in H^1(\Omega), \|\varphi\|_{H^1(\Omega)} = 1} \langle \partial_t v, \varphi \rangle = \sup_{\varphi \in H^1(\Omega)} \frac{\langle \partial_t v, \varphi \rangle}{\|\varphi\|_{H^1(\Omega)}}.$$

For the sake of completeness, we also recall the Gronwall Lemma that will be used in the sequel.

Lemma 4.5 (Gronwall's Lemma). *Let φ and $y : [a, b] \to \mathbb{R}_+$ be two continuous functions satisfying*

$$\exists C \geq 0, \forall t \in [a, b], \ y'(t) \leq C + \int_a^t \varphi(s) y(s) \, \mathrm{ds}.$$

Then, for all $t \in [a, b]$ we have

$$y(t) \leq C e^{\int_a^t \varphi(s) \, \mathrm{ds}}.$$

The residuals associated to (2.4) are defined by

$$
\begin{aligned}
&\langle \mathcal{R}_1(v_{h\tau}^k), \varphi \rangle_{X', X} \\
&= \int_0^T \left\{ -\left(\partial_t v_{h\tau}^k, \varphi\right)_\Omega - (\Lambda \boldsymbol{\nabla} v_{h\tau}^k, \boldsymbol{\nabla}\varphi)_\Omega - \langle f(v_{h\tau}^k, w_{h\tau}^k), \varphi \rangle \right\} (t) \, \mathrm{dt}
\end{aligned}
\tag{4.12}
$$

$$\langle \mathcal{R}_2(w_{h\tau}^k), \psi \rangle_{Y, Y} = -\int_0^T \left\{ \left(\partial_t w_{h\tau}^k, \psi\right)_\Omega - \left(g(v_{h\tau}^k, w_{h\tau}^k), \psi\right)_\Omega \right\} (t) \, \mathrm{dt} \tag{4.13}$$

for $\varphi \in X$ and $\psi \in Y$. The dual norm of the residuals is naturally defined by

$$
\begin{aligned}
\| |\mathcal{R}_1(v_{h\tau}^k)| \|_{X'} &= \sup_{\varphi \in X} \frac{|\langle \mathcal{R}_1(v_{h\tau}^k), \varphi \rangle_{X', X}|}{\|\varphi\|_X} \\
\| |\mathcal{R}_2(w_{h\tau})| \|_Y &= \sup_{\psi \in Y} \frac{|\langle \mathcal{R}_2(w_{h\tau}^k), \psi \rangle_{Y, Y}|}{\|\psi\|_Y}.
\end{aligned}
\tag{4.14}
$$

Proposition 4.6. *Let* $(v, w) \in X \times Y$ *be the solution of* (2.4) *and let* $(v_{h\tau}^k, w_{h\tau}^k) \in X_h^p \times X_h^p$ *be the approximate solution. Assume that* f *is* K_f-*Lipschitz and* g *is* K_g-*Lipschitz. We have*

$$\left\| \mathcal{R}_1(v_{h\tau}^k) \right\|_{X'} \leq \left\| \partial_t(v - v_{h\tau}^k) \right\|_Y + \left\| v - v_{h\tau}^k \right\|_X + K_f \left(\left\| v - v_{h\tau}^k \right\|_Y + \left\| w - w_{h\tau}^k \right\|_Y \right)$$

$$\left\| \mathcal{R}_2(w_{h\tau}^k) \right\|_Y \leq \left\| \partial_t(w - w_{h\tau}^k) \right\|_Y + K_g \left(\left\| v - v_{h\tau}^k \right\|_Y + \left\| w - w_{h\tau}^k \right\|_Y \right).$$

Proof. Employing System (2.4) together with the expressions of the residual $\mathcal{R}_1$ we have, $\forall \varphi \in X$,

$$\int_0^T \left(\partial_t(v - v_{h\tau}^k), \varphi \right)_\Omega (t) \, \mathrm{d}t + \int_0^T \left(\Lambda \boldsymbol{\nabla} \left(v - v_{h\tau}^k \right), \boldsymbol{\nabla} \varphi \right)_\Omega (t) \, \mathrm{d}t$$

$$+ \int_0^T \left\langle f(v, w) - f(v_{h\tau}^k, w_{h\tau}^k), \varphi \right\rangle (t) \, \mathrm{d}t = \left\langle \mathcal{R}_1(v_{h\tau}^k), \varphi \right\rangle.$$

The Cauchy–Schwarz inequality gives

$$| \left\langle \mathcal{R}_1(v_{h\tau}^k), \varphi \right\rangle_{X', X} | \leq \left\| \partial_t(v - v_{h\tau}^k) \right\|_Y \|\varphi\|_Y + \left\| \Lambda^{\frac{1}{2}} \boldsymbol{\nabla}(v - v_{h\tau}^k) \right\|_Y \|\boldsymbol{\nabla}\varphi\|_Y$$

$$+ \left\| f(v, w) - f(v_{h\tau}^k, w_{h\tau}^k) \right\|_{X'} \|\varphi\|_X.$$

Next we use the fact that $\|\varphi\|_Y \leq \|\varphi\|_X$ and $\|\boldsymbol{\nabla}\varphi\|_Y \leq \|\varphi\|_X$, so we get

$$| \left\langle \mathcal{R}_1(v_{h\tau}^k), \varphi \right\rangle_{X', X} | \leq \left(\left\| \partial_t(v - v_{h\tau}^k) \right\|_Y + \left\| \Lambda^{\frac{1}{2}} \boldsymbol{\nabla}(v - v_{h\tau}^k) \right\|_Y \right) \|\varphi\|_X$$

$$+ \left\| f(v, w) - f(v_{h\tau}^k, w_{h\tau}^k) \right\|_{X'} \|\varphi\|_X.$$

Nevertheless, the Lipschitz behavior of f implies that

$$| \left\langle \mathcal{R}_1(v_{h\tau}^k), \varphi \right\rangle_{X', X} | \leq \left(\left\| \partial_t(v - v_{h\tau}^k) \right\|_Y + \left\| \Lambda^{\frac{1}{2}} \boldsymbol{\nabla}(v - v_{h\tau}^k) \right\|_Y \right) \|\varphi\|_X$$

$$+ K_f \left(\left\| v - v_{h\tau}^k \right\|_Y + \left\| w - w_{h\tau}^k \right\|_Y \right) \|\varphi\|_X.$$

Thus

$$\left\| \mathcal{R}_1(v_{h\tau}^k) \right\|_{X'} \leq \left\| \partial_t(v - v_{h\tau}^k) \right\|_Y + \left\| v - v_{h\tau}^k \right\|_X$$

$$+ K_f \left(\left\| v - v_{h\tau}^k \right\|_Y + \left\| w - w_{h\tau}^k \right\|_Y \right).$$

Employing the same arguments we have

$$\int_0^T \left(\partial_t(w - w_{h\tau}^k), \psi \right)_\Omega (t) \, \mathrm{d}t + \int_0^T \left(g(v, w) - g(v_{h\tau}^k, w_{h\tau}^k), \psi \right)_\Omega (t) \, \mathrm{d}t$$

$$= \left\langle \mathcal{R}_2(w_{h\tau}^k), \psi \right\rangle_{Y, Y}$$

and then

$$| \left\langle \mathcal{R}_2(w_{h\tau}^k), \psi \right\rangle_{Y, Y} | \leq \left\| \partial_t(w - w_{h\tau}^k) \right\|_Y \|\psi\|_Y$$

$$+ K_g \left(\left\| v - v_{h\tau}^k \right\|_Y + \left\| w - w_{h\tau}^k \right\|_Y \right) \|\psi\|_Y.$$

Therefore,

$$\left\| \mathcal{R}_2(w_{h\tau}^k) \right\|_Y \leq \left\| \partial_t(w - w_{h\tau}^k) \right\|_Y + K_g \left(\left\| v - v_{h\tau}^k \right\|_Y + \left\| w - w_{h\tau}^k \right\|_Y \right).$$

$\square$

Proposition 4.7. *Let* $(v, w) \in X \times Y$ *be the solution of* (2.4) *and let* $(v_{h\tau}^k, w_{h\tau}^k) \in X_h^p \times X_h^p$ *be the approximate solution. Consider the conditions listed in Assumption 2.2. Then,*

$$\left\| v - v_{h\tau}^k \right\|_X^2 + \left\| \partial_t(v - v_{h\tau}^k) \right\|_Y^2 + \left\| w - w_{h\tau}^k \right\|_Y^2 + \left\| \partial_t(w - w_{h\tau}^k) \right\|_Y^2$$

$$\leq C_\star \left(\left\| \mathcal{R}_1(v_{h\tau}^k) \right\|_Y^2 + \left\| \mathcal{R}_2(w_{h\tau}^k) \right\|_Y^2 \right. \tag{4.15}$$

$$\left. + \left\| (v - v_{h\tau}^k)(\cdot, 0) \right\|_\Omega^2 + \alpha_4 \left\| (w - w_{h\tau}^k)(\cdot, 0) \right\|_\Omega^2 \right)$$

where $C_\star$ *is a generic constant that depends on* Ω, f, g *and* T.

13

Proof. Employing System (2.4) together with the expressions of the residuals $\mathcal{R}_1(v_{h\tau}^k)$ and $\mathcal{R}_2(w_{h\tau}^k)$ given by (4.12) and (4.13) we have, $\forall \varphi \in X, \forall \psi \in Y$,

$$
\int_0^T \left(\partial_t (v - v_{h\tau}^k), \varphi \right)_\Omega (t) \, \mathrm{dt} + \int_0^T \left(\Lambda \boldsymbol{\nabla} \left(v - v_{h\tau}^k \right), \boldsymbol{\nabla} \varphi \right)_\Omega (t) \, \mathrm{dt}
$$
$$
+ \int_0^T \left\langle f(v, w) - f(v_{h\tau}^k, w_{h\tau}^k), \varphi \right\rangle (t) \, \mathrm{dt} + \int_0^T \left(\partial_t (w - w_{h\tau}^k), \psi \right)_\Omega (t) \, \mathrm{dt} \tag{4.16}
$$
$$
+ \int_0^T \left(g(v, w) - g(v_{h\tau}^k, w_{h\tau}^k), \psi \right)_\Omega (t) \, \mathrm{dt} = \left\langle \mathcal{R}_1(v_{h\tau}^k), \varphi \right\rangle_{X', X} + \left\langle \mathcal{R}_2(w_{h\tau}^k), \psi \right\rangle_{Y, Y}.
$$

Next, we substitute $\varphi = v - v_{h\tau}^k \in X$ and $\psi = \alpha_4 \left(w - w_{h\tau}^k \right) \in Y$ in (4.16) and employing [33, Theorem 5.9.3] to obtain

$$
\frac{1}{2} \left(\left\| (v - v_{h\tau}^k)(\cdot, T) \right\|_\Omega^2 - \left\| (v - v_{h\tau}^k)(\cdot, 0) \right\|_\Omega^2 + \alpha_4 \left\| (w - w_{h\tau}^k)(\cdot, T) \right\|_\Omega^2 \right.
$$
$$
\left. - \alpha_4 \left\| (w - w_{h\tau}^k)(\cdot, 0) \right\|_\Omega^2 \right) + \int_0^T \left(\Lambda \boldsymbol{\nabla} \left(v - v_{h\tau}^k \right), \boldsymbol{\nabla} \left(v - v_{h\tau}^k \right) \right)_\Omega (t) \, \mathrm{dt}
$$
$$
+ \int_0^T \left\langle f(v, w) - f(v_{h\tau}^k, w_{h\tau}^k), v - v_{h\tau}^k \right\rangle (t) \, \mathrm{dt}
$$
$$
+ \int_0^T \alpha_4 \left(g(v, w) - g(v_{h\tau}^k, w_{h\tau}^k), w - w_{h\tau}^k \right)_\Omega (t) \, \mathrm{dt}
$$
$$
= \left\langle \mathcal{R}_1(v_{h\tau}^k), v - v_{h\tau}^k \right\rangle_{X', X} + \left\langle \mathcal{R}_2(w_{h\tau}^k), w - w_{h\tau}^k \right\rangle_{Y, Y}.
$$

which is equivalent (using the linearity of f_2 and the bilinearity of g) to

$$
\frac{1}{2} \left[\left\| (v - v_{h\tau}^k)(\cdot, T) \right\|_\Omega^2 + \alpha_4 \left\| (w - w_{h\tau}^k)(\cdot, T) \right\|_\Omega^2 \right] + \left\| v - v_{h\tau}^k \right\|_X^2
$$
$$
+ \int_0^T \left(\tilde{f}_1(v) - \tilde{f}_1(v_{h\tau}^k), v - v_{h\tau}^k \right)_\Omega (t) \, \mathrm{dt}
$$
$$
+ \int_0^T \left(\left(f_2 \left(w - w_{h\tau}^k \right), v - v_{h\tau}^k \right)_\Omega + \alpha_4 \left(g \left(v - v_{h\tau}^k, w - w_{h\tau}^k \right), w - w_{h\tau}^k \right)_\Omega \right) (t) \, \mathrm{dt} \tag{4.17}
$$
$$
= \left\langle \mathcal{R}_1(v_{h\tau}^k), v - v_{h\tau}^k \right\rangle_{X', X} + \left\langle \mathcal{R}_2(w_{h\tau}^k), w - w_{h\tau}^k \right\rangle_{Y, Y}
$$
$$
+ (\beta_1 + 1) \int_0^T \left\| v - v_{h\tau}^k \right\|_\Omega^2 (t) \, \mathrm{dt}
$$
$$
+ \frac{1}{2} \left[\left\| (v - v_{h\tau}^k)(\cdot, 0) \right\|_\Omega^2 + \alpha_4 \left\| (w - w_{h\tau}^k)(\cdot, 0) \right\|_\Omega^2 \right].
$$

Then, equation (4.17) reads as

$$
E_1 + E_2 + E_3 + E_4 = E_5 + E_6 + E_7 + E_8
$$

with

$$
E_1 := \frac{1}{2} \left[\left\| (v - v_{h\tau}^k)(\cdot, T) \right\|_\Omega^2 + \alpha_4 \left\| (w - w_{h\tau}^k)(\cdot, T) \right\|_\Omega^2 \right], \quad E_2 := \left\| v - v_{h\tau}^k \right\|_X^2
$$
$$
E_3 := \int_0^T \left(\tilde{f}_1(v) - \tilde{f}_1(v_{h\tau}^k), v - v_{h\tau}^k \right)_\Omega (t) \, \mathrm{dt}
$$
$$
E_4 := \int_0^T \left(\left(f_2 \left(w - w_{h\tau}^k \right), v - v_{h\tau}^k \right)_\Omega + \alpha_4 \left(g \left(v - v_{h\tau}^k, w - w_{h\tau}^k \right), w - w_{h\tau}^k \right)_\Omega \right) (t) \, \mathrm{dt}
$$
$$
E_5 := \left\langle \mathcal{R}_1(v_{h\tau}^k), v - v_{h\tau}^k \right\rangle_{X', X}, \quad E_6 := \left\langle \mathcal{R}_2(w_{h\tau}^k), w - w_{h\tau}^k \right\rangle_{Y, Y}
$$
$$
E_7 := (\beta_1 + 1) \int_0^T \left\| v - v_{h\tau}^k \right\|_\Omega^2 (t) \, \mathrm{dt},
$$
$$
E_8 := \frac{1}{2} \left[\left\| (v - v_{h\tau}^k)(\cdot, 0) \right\|_\Omega^2 + \alpha_4 \left\| (w - w_{h\tau}^k)(\cdot, 0) \right\|_\Omega^2 \right].
$$

Now, we estimate E_i with $i = 3, \ldots, 7$ as follows. Using Assumption 2.2 on $\tilde{f}_1$, we deduce that

$$E_3 \geq 0. \tag{4.18}$$

Using again Assumption 2.1 this time on f_2 and g, we obtain

$$E_4 \geq \alpha_5 \left\| w - w_{h\tau} \right\|_Y^2. \tag{4.19}$$

As a result of the Cauchy–Schwarz inequality and the Young inequality, we get

$$E_5 + E_6 \leq \frac{1}{2} \left(\left\|\left| \mathcal{R}_1(v_{h\tau}^k) \right|\right\|_{X'}^2 + \left\|\left| \mathcal{R}_2(w_{h\tau}^k) \right|\right\|_Y^2 \right) + \frac{1}{2} \left(\left\| v - v_{h\tau}^k \right\|_X^2 + \left\| w - w_{h\tau}^k \right\|_Y^2 \right). \tag{4.20}$$

Using the definition of E_7 and applying the Cauchy–Schwarz inequality, we get the following bound

$$E_7 \leq (\beta_1 + 1) \int_0^T \left\| v - v_{h\tau}^k \right\|_\Omega^2 (t) \, \mathrm{dt}. \tag{4.21}$$

Combining (4.18), (4.19), (4.20), (4.21) with (4.17) we obtain

$$\begin{aligned}
&\frac{1}{2} \left[\left\| (v - v_{h\tau}^k)(\cdot, T) \right\|_\Omega^2 + \alpha_4 \left\| (w - w_{h\tau}^k)(\cdot, T) \right\|_\Omega^2 \right] + \frac{1}{2} \left\| v - v_{h\tau}^k \right\|_X^2 + \alpha_5 \left\| w - w_{h\tau}^k \right\|_Y^2 \\
&\leq \frac{1}{2} \left(\left\|\left| \mathcal{R}_1(v_{h\tau}^k) \right|\right\|_{X'}^2 + \left\|\left| \mathcal{R}_2(w_{h\tau}^k) \right|\right\|_Y^2 + \left\| (v - v_{h\tau}^k)(\cdot, 0) \right\|_\Omega^2 + \alpha_4 \left\| (w - w_{h\tau}^k)(\cdot, 0) \right\|_\Omega^2 \right) \\
&\quad + \max \left\{ \beta_1 + 1, \frac{1}{2} \right\} \left[\int_0^T \left\| v - v_{h\tau}^k \right\|_\Omega^2 (t) \, \mathrm{dt} + \int_0^T \left\| w - w_{h\tau}^k \right\|_\Omega^2 (t) \, \mathrm{dt} \right].
\end{aligned} \tag{4.22}$$

It immediately follows that

$$\begin{aligned}
&\left\| (v - v_{h\tau}^k)(\cdot, T) \right\|_\Omega^2 + \alpha_4 \left\| (w - w_{h\tau}^k)(\cdot, T) \right\|_\Omega^2 \\
&\leq \left\|\left| \mathcal{R}_1(v_{h\tau}^k) \right|\right\|_{X'}^2 + \left\|\left| \mathcal{R}_2(w_{h\tau}^k) \right|\right\|_Y^2 + \left\| (v - v_{h\tau}^k)(\cdot, 0) \right\|_\Omega^2 + \alpha_4 \left\| (w - w_{h\tau}^k)(\cdot, 0) \right\|_\Omega^2 \\
&\quad + 2 (\beta_1 + 1) \max \left\{ 1, \frac{1}{\alpha_4} \right\} \left[\int_0^T \left(\left\| v - v_{h\tau}^k \right\|_\Omega^2 + \alpha_4 \left\| w - w_{h\tau}^k \right\|_\Omega^2 \right) (t) \, \mathrm{dt} \right].
\end{aligned}$$

As a result of Gronwall's Lemma 4.5 and setting $\widetilde{C} := 2T(\beta_1 + 1) \max \left\{ 1, \dfrac{1}{\alpha_4} \right\}$ we find

$$\begin{aligned}
&\left\| (v - v_{h\tau}^k)(\cdot, T) \right\|_\Omega^2 + \alpha_4 \left\| (w - w_{h\tau}^k)(\cdot, T) \right\|_\Omega^2 \\
&\leq e^{\widetilde{C}} \left(\left\|\left| \mathcal{R}_1(v_{h\tau}^k) \right|\right\|_{X'}^2 + \left\|\left| \mathcal{R}_2(w_{h\tau}^k) \right|\right\|_Y^2 + \left\| (v - v_{h\tau}^k)(\cdot, 0) \right\|_\Omega^2 + \alpha_4 \left\| (w - w_{h\tau}^k)(\cdot, 0) \right\|_\Omega^2 \right).
\end{aligned}$$

Hence, we deduce that

$$\begin{aligned}
&\left\| v - v_{h\tau}^k \right\|_{L^\infty(0,T;L^2(\Omega))}^2 + \alpha_4 \left\| w - w_{h\tau}^k \right\|_{L^\infty(0,T;L^2(\Omega))}^2 \\
&\leq e^{\widetilde{C}} \left(\left\|\left| \mathcal{R}_1(v_{h\tau}^k) \right|\right\|_{X'}^2 + \left\|\left| \mathcal{R}_2(w_{h\tau}^k) \right|\right\|_Y^2 + \left\| (v - v_{h\tau}^k)(\cdot, 0) \right\|_\Omega^2 + \alpha_4 \left\| (w - w_{h\tau}^k)(\cdot, 0) \right\|_\Omega^2 \right).
\end{aligned}$$

Moreover, one can obtain from (4.22) the following estimate on $\left\| v - v_{h\tau}^k \right\|_X$ and $\left\| w - w_{h\tau}^k \right\|_Y$

$$\begin{aligned}
&\left\| v - v_{h\tau}^k \right\|_X^2 + 2\alpha_5 \left\| w - w_{h\tau}^k \right\|_Y^2 \\
&\leq \left\|\left| \mathcal{R}_1(v_{h\tau}^k) \right|\right\|_{X'}^2 + \left\|\left| \mathcal{R}_2(w_{h\tau}^k) \right|\right\|_Y^2 + \left\| (v - v_{h\tau}^k)(\cdot, 0) \right\|_\Omega^2 \\
&\quad + \alpha_4 \left\| (w - w_{h\tau}^k)(\cdot, 0) \right\|_\Omega^2 \\
&\quad + \widetilde{C} \left[\left\| v - v_{h\tau}^k \right\|_{L^\infty(0,T;L^2(\Omega))}^2 + \alpha_4 \left\| w - w_{h\tau}^k \right\|_{L^\infty(0,T;L^2(\Omega))}^2 \right].
\end{aligned} \tag{4.23}$$

Finally, we take $\psi = 0$ in (4.16), to get

$$\int_0^T \left(\partial_t(v - v_{h\tau}^k), \varphi\right)_\Omega (t) \, \mathrm{dt} + \int_0^T \left(\Lambda\boldsymbol{\nabla}\left(v - v_{h\tau}^k\right), \boldsymbol{\nabla}\varphi\right)_\Omega (t) \, \mathrm{dt}$$
$$+ \int_0^T \left\langle f(v,w) - f(v_{h\tau}^k, w_{h\tau}^k), \varphi \right\rangle (t) \, \mathrm{dt} = \left\langle \mathcal{R}_1(v_{h\tau}^k), \varphi \right\rangle_{X',X}.$$

Then, using the Cauchy–Schwarz inequality and the Lipshitz behavior of the function f we obtain

$$\begin{aligned}
\left\|\partial_t\left(v - v_{h\tau}^k\right)\right\|_Y &\leq \left\|\!\left\|\mathcal{R}_1(v_{h\tau}^k)\right\|\!\right\|_{X'} + \left\|v - v_{h\tau}^k\right\|_X \\
&\quad + K_f\sqrt{T}\widetilde{\alpha}_4\left(\left\|v - v_{h\tau}^k\right\|_{L^\infty(0,T;L^2(\Omega))} + \sqrt{\alpha_4}\left\|w - w_{h\tau}^k\right\|_{L^\infty(0,T;L^2(\Omega))}\right)
\end{aligned} \tag{4.24}$$

with $\widetilde{\alpha}_4 = \max\left\{1, \frac{1}{\sqrt{\alpha_4}}\right\}$. Similarly, taking $\phi = 0$ in (4.16) we get,

$$\int_0^T \left(\partial_t(w - w_{h\tau}^k) + g(v,w) - g(v_{h\tau}^k, w_{h\tau}^k), \psi\right)_\Omega (t) \, \mathrm{dt} = \left\langle \mathcal{R}_2(w_{h\tau}^k), \psi \right\rangle_{X',X}.$$

Employing the Cauchy–Schwarz inequality we get

$$\left\|\partial_t(w - w_{h\tau}^k)\right\|_Y \|\psi\|_Y \leq \left\|\!\left\|\mathcal{R}_2(w_{h\tau}^k)\right\|\!\right\|_Y \|\psi\|_Y + \left\|g(v,w) - g(v_{h\tau}^k, w_{h\tau}^k)\right\|_Y \|\psi\|_Y.$$

Therefore, we have thanks to the Lipschitz behavior of the function g,

$$\begin{aligned}
\left\|\partial_t(w - w_{h\tau}^k)\right\|_Y &\leq \left\|\!\left\|\mathcal{R}_2(w_{h\tau}^k)\right\|\!\right\|_Y \\
&\quad + K_g\sqrt{T}\widetilde{\alpha}_4\left(\left\|v - v_{h\tau}^k\right\|_{L^\infty(0,T;L^2(\Omega))} + \sqrt{\alpha_4}\left\|w - w_{h\tau}^k\right\|_{L^\infty(0,T;L^2(\Omega))}\right).
\end{aligned} \tag{4.25}$$

Combining (4.23), (4.24) and (4.25), we get

$$\begin{aligned}
&\left\|v - v_{h\tau}^k\right\|_X^2 + \left\|\partial_t(v - v_{h\tau}^k)\right\|_Y^2 + 2\alpha_5\left\|w - w_{h\tau}^k\right\|_Y^2 + \left\|\partial_t(w - w_{h\tau}^k)\right\|_Y^2 \\
&\leq C\left(\left\|\!\left\|\mathcal{R}_1(v_{h\tau}^k)\right\|\!\right\|_{X'}^2 + \left\|\!\left\|\mathcal{R}_2(w_{h\tau}^k)\right\|\!\right\|_Y^2 + \left\|(v - v_{h\tau}^k)(\cdot, 0)\right\|_\Omega^2 + \alpha_4\left\|(w - w_{h\tau}^k)(\cdot, 0)\right\|_\Omega^2\right)
\end{aligned}$$

with $C = 6 + \left[\widetilde{C} + \left(6K_f^2 + 4K_g^2\right)\widetilde{\alpha}_4^2 T\right]e^{\widetilde{C}}$. Hence, we obtain the desired estimate with $C_\star = \dfrac{C\max\{1, \alpha_4\}}{\min\{1, 2\alpha_5\}}$. $\qquad\square$

4.5 A posteriori error estimates

In this section, for any polynomial degree $p \geq 1$, we derive an a posteriori error estimate on the error between the exact solution (v, w) given by the weak formulation (2.4) and the approximate solution $\left(v_h^{n,k}, w_h^{n,k}\right)$ given by (3.2) which is valid at any time step $1 \leq n \leq N_t$ and any Newton step $k \geq 1$.

Theorem 4.8. *Let (v, w) be the solution of the continuous problem (2.1). Let $\left(v_{h\tau}^k, w_{h\tau}^k\right)$ be the approximate solution stemming from the exact linearization solver at each time step $1 \leq n \leq N_t$. Let $\boldsymbol{\sigma}_{h\tau,\mathrm{tot}}^k \in L^2(0, T; \boldsymbol{H}(\mathrm{div}, \Omega))$ be the equilibrated flux reconstruction satisfying (4.5). Let finally $K \in \mathcal{T}_h$ and define the residual estimators by*

$$\begin{aligned}
\eta_{\mathrm{R}_1,K}^{n,k}(t) &:= C_{\mathrm{P},K}h_K\left\|\partial_t v_{h\tau}^{n,k} + \mathcal{F}(v_{h\tau}^{n,k}, w_{h\tau}^{n,k}) + \boldsymbol{\nabla}\cdot\boldsymbol{\sigma}_{h\tau,\mathrm{tot}}^{n,k}\right\|_K (t) \\
\eta_{\mathrm{R}_2,K}^{n,k}(t) &:= \left\|\partial_t w_{h\tau}^{n,k} + g\left(v_{h\tau}^{n,k}, w_{h\tau}^{n,k}\right)\right\|_K (t)
\end{aligned} \tag{4.26}$$

the flux estimator by

$$\eta_{\mathrm{F},K}^{n,k}(t) := \left\|\Lambda\boldsymbol{\nabla}v_{h\tau}^{n,k} + \boldsymbol{\sigma}_{h\tau,\mathrm{tot}}^{n,k}\right\|_K (t) \tag{4.27}$$

the linearization estimator by

$$\eta_{\text{lin},1,K}^{n,k} := \left\| \mathcal{F}(v_{h\tau}^{n,k}, w_{h\tau}^{n,k}) - f(v_{h\tau}^{n,k}, w_{h\tau}^{n,k}) \right\|_K (t) \tag{4.28}$$

and the initial condition estimators by

$$\eta_{\text{IC},1,K}^k := \left\| (v - v_{h\tau}^k)(\cdot, 0) \right\|_K, \quad \eta_{\text{IC},2,K}^k := \sqrt{\alpha_4} \left\| (w - w_{h\tau}^k)(\cdot, 0) \right\|_K. \tag{4.29}$$

Then, the following a posteriori error estimate holds,

$$\frac{1}{2\sqrt{C_\star}} \left(\left\| \partial_t \left(w - w_{h\tau}^{n,k} \right) \right\|_Y + \left\| w - w_{h\tau}^{n,k} \right\|_Y + \left\| \partial_t \left(v - v_{h\tau}^{n,k} \right) \right\|_Y + \left\| v - v_{h\tau}^{n,k} \right\|_X \right) \leq \eta^k$$

with the global estimator η^k defined by

$$\eta^k := \left\{ \sum_{n=1}^{N_t} \int_{I_n} \sum_{K \in \mathcal{T}_h} \left(\left(\eta_{\text{R}_1,K}^{n,k} + \eta_{\text{F},K}^{n,k} + \eta_{\text{lin},1,K}^{n,k} \right)^2 + \left(\eta_{\text{R}_2,K}^{n,k} \right)^2 \right) (t) \, \text{dt} \right.$$
$$\left. + \sum_{K \in \mathcal{T}_h} \left(\left(\eta_{\text{IC},1,K}^k \right)^2 + \left(\eta_{\text{IC},2,K}^k \right)^2 \right) \right\}^{\frac{1}{2}}. \tag{4.30}$$

Proof. Using (4.15) it is enough to bound the term $\left\| \mathcal{R}_1(v_{h\tau}^k) \right\|_{X'}$ and $\left\| \mathcal{R}_2(w_{h\tau}^k) \right\|_Y$ to get the desired result. First, employing the defintion (4.14) we have

$$\left\| \mathcal{R}_1(v_{h\tau}^k) \right\|_{X'} = \sup_{\varphi \in X, \|\varphi\|_X = 1} \int_0^T \left\{ - \left(\partial_t v_{h\tau}^k + f(v_{h\tau}^k, w_{h\tau}^k), \varphi \right)_\Omega - (\Lambda \boldsymbol{\nabla} v_{h\tau}^k, \boldsymbol{\nabla} \varphi)_\Omega \right\} (t) \, \text{dt}.$$

Adding and subtracting $\boldsymbol{\nabla} \cdot \boldsymbol{\sigma}_{h\tau,\text{tot}}^k$ and using afterwards the Green-formula (since $\boldsymbol{\sigma}_{h\tau,\text{tot}} \in L^2(0, T; \mathbf{H}(\text{div}, \Omega))$ and $\varphi \in X$) we get

$$\left\| \mathcal{R}_1(v_{h\tau}^k) \right\|_{X'} = \sup_{\varphi \in X, \|\varphi\|_X = 1} \sum_{n=1}^{N_t} \int_{I_n} \sum_{K \in \mathcal{T}_h} \left\{ - \left(\partial_t v_{h\tau}^{n,k} + f(v_{h\tau}^{n,k}, w_{h\tau}^{n,k}) + \boldsymbol{\nabla} \cdot \boldsymbol{\sigma}_{h\tau,\text{tot}}^{n,k}, \varphi \right)_K \right.$$
$$\left. - (\Lambda \boldsymbol{\nabla} v_{h\tau}^{n,k} + \boldsymbol{\sigma}_{h\tau,\text{tot}}^{n,k}, \boldsymbol{\nabla} \varphi)_K \right\} (t) \, \text{dt}.$$

We add the linearized source term $\mathcal{F}(v_{h\tau}^{n,k}, w_{h\tau}^{n,k})$ so that

$$\left\| \mathcal{R}_1(v_{h\tau}^k) \right\|_{X'} = \sup_{\varphi \in X, \|\varphi\|_X = 1} \sum_{n=1}^{N_t} \int_{I_n} \sum_{K \in \mathcal{T}_h} \left\{ - \left(\partial_t v_{h\tau}^{n,k} + \mathcal{F}(v_{h\tau}^{n,k}, w_{h\tau}^{n,k}) + \boldsymbol{\nabla} \cdot \boldsymbol{\sigma}_{h\tau,\text{tot}}^{n,k}, \varphi \right)_K \right.$$
$$\left. - (\Lambda \boldsymbol{\nabla} v_{h\tau}^{n,k} + \boldsymbol{\sigma}_{h\tau,\text{tot}}^{n,k}, \boldsymbol{\nabla} \varphi)_K + \left(\mathcal{F}(v_{h\tau}^{n,k}, w_{h\tau}^{n,k}) - f(v_{h\tau}^{n,k}, w_{h\tau}^{n,k}), \varphi \right)_K \right\} (t) \, \text{dt}.$$

Next, as a result of (4.7) we observe that

$$- \left(\partial_t v_{h\tau}^{n,k} + \mathcal{F}(v_{h\tau}^{n,k}, w_{h\tau}^{n,k}) + \boldsymbol{\nabla} \cdot \boldsymbol{\sigma}_{h\tau,\text{tot}}^{n,k}, \varphi \right)_K$$
$$= - \left(\partial_t v_{h\tau}^{n,k} + \mathcal{F}(v_{h\tau}^{n,k}, w_{h\tau}^{n,k}) + \boldsymbol{\nabla} \cdot \boldsymbol{\sigma}_{h\tau,\text{tot}}^{n,k}, \varphi - \overline{\varphi}_K \right)_K.$$

Besides, the Cauchy–Schwarz and next the Poincaré–Wirtinger inequalities give

$$- \left(\partial_t v_{h\tau}^{n,k} + \mathcal{F}(v_{h\tau}^{n,k}, w_{h\tau}^{n,k}) + \boldsymbol{\nabla} \cdot \boldsymbol{\sigma}_{h\tau,\text{tot}}^{n,k}, \varphi - \overline{\varphi}_K \right)_K \leq \eta_{\text{R}_1,K}^{n,k} \left\| \boldsymbol{\nabla} \varphi \right\|_K. \tag{4.31}$$

Furthermore, applying again the Cauchy–Schwarz inequality we obtain

$$-(\Lambda \boldsymbol{\nabla} v_{h\tau}^{n,k} + \boldsymbol{\sigma}_{h\tau,\text{tot}}^{n,k}, \boldsymbol{\nabla} \varphi)_K \leq \eta_{\text{F},K}^{n,k} \left\| \boldsymbol{\nabla} \varphi \right\|_K. \tag{4.32}$$

17

and also
$$\left(\mathcal{F}(v_{h\tau}^{n,k}, w_{h\tau}^{n,k}) - f(v_{h\tau}^{n,k}, w_{h\tau}^{n,k}), \varphi\right)_K \leq \eta_{\mathrm{lin},1,K}^{n,k} \|\varphi\|_K. \tag{4.33}$$

Finally combining (4.31), (4.32) and (4.33) we get

$$
\begin{aligned}
&- \sum_{K \in \mathcal{T}_h} \left(\partial_t v_{h\tau}^{n,k} + \mathcal{F}(v_{h\tau}^{n,k}, w_{h\tau}^{n,k}) + \boldsymbol{\nabla} \cdot \boldsymbol{\sigma}_{h\tau,\mathrm{tot}}^{n,k}, \varphi\right)_K - \sum_{K \in \mathcal{T}_h} (\Lambda \boldsymbol{\nabla} v_{h\tau}^{n,k} + \boldsymbol{\sigma}_{h\tau,\mathrm{tot}}^{n,k}, \boldsymbol{\nabla}\varphi)_K \\
&+ \sum_{K \in \mathcal{T}_h} \left(\mathcal{F}(v_{h\tau}^{n,k}, w_{h\tau}^{n,k}) - f(v_{h\tau}^{n,k}, w_{h\tau}^{n,k}), \varphi\right)_K \\
&\leq \sum_{K \in \mathcal{T}_h} \left(\eta_{\mathrm{R}_1,K}^{n,k} + \eta_{\mathrm{F},K}^{n,k}\right) \|\boldsymbol{\nabla}\varphi\|_K + \sum_{K \in \mathcal{T}_h} \eta_{\mathrm{lin},1,K}^{n,k} \|\varphi\|_K \\
&\leq \sum_{K \in \mathcal{T}_h} \left(\eta_{\mathrm{R}_1,K}^{n,k} + \eta_{\mathrm{F},K}^{n,k} + \eta_{\mathrm{lin},1,K}^{n,k}\right) \max\left\{\|\varphi\|_K, \|\boldsymbol{\nabla}\varphi\|_K\right\}.
\end{aligned}
$$

The Cauchy–Schwarz inequality gives

$$
\begin{aligned}
&- \sum_{K \in \mathcal{T}_h} \left(\partial_t v_{h\tau}^{n,k} + \mathcal{F}(v_{h\tau}^{n,k}, w_{h\tau}^{n,k}) + \boldsymbol{\nabla} \cdot \boldsymbol{\sigma}_{h\tau,\mathrm{tot}}^{n,k}, \varphi\right)_K - \sum_{K \in \mathcal{T}_h} (\Lambda \boldsymbol{\nabla} v_{h\tau}^{n,k} + \boldsymbol{\sigma}_{h\tau,\mathrm{tot}}^{n,k}, \boldsymbol{\nabla}\varphi)_K \\
&+ \sum_{K \in \mathcal{T}_h} \left(\mathcal{F}(v_{h\tau}^{n,k}, w_{h\tau}^{n,k}) - f(v_{h\tau}^{n,k}, w_{h\tau}^{n,k}), \varphi\right)_K \\
&\leq \left\{\sum_{K \in \mathcal{T}_h} \left(\eta_{\mathrm{R}_1,K}^{n,k} + \eta_{\mathrm{F},K}^{n,k} + \eta_{\mathrm{lin},1,K}^{n,k}\right)^2\right\}^{\frac{1}{2}} \max\left\{\|\varphi\|_\Omega, \|\boldsymbol{\nabla}\varphi\|_\Omega\right\}.
\end{aligned}
$$

Hence, we obtain the estimate on $\left|\!\left|\!\left|\mathcal{R}_1(v_{h\tau}^k)\right|\!\right|\!\right|_{X'}$ thanks to the Cauchy–Schwarz inequality

$$\left|\!\left|\!\left|\mathcal{R}_1(v_{h\tau}^k)\right|\!\right|\!\right|_{X'} \leq \left\{\sum_{n=1}^{N_t} \int_{I_n} \sum_{K \in \mathcal{T}_h} \left(\eta_{\mathrm{R}_1,K}^{n,k} + \eta_{\mathrm{F},K}^{n,k} + \eta_{\mathrm{lin},1,K}^{n,k}\right)^2 (t)\, \mathrm{dt}\right\}^{\frac{1}{2}}. \tag{4.34}$$

Similarly, we can obtain an analogous estimate on $\left|\!\left|\!\left|\mathcal{R}_2(w_{h\tau}^k)\right|\!\right|\!\right|_Y$

$$\left|\!\left|\!\left|\mathcal{R}_2(w_{h\tau}^k)\right|\!\right|\!\right|_Y \leq \left\{\sum_{n=1}^{N_t} \int_{I_n} \sum_{K \in \mathcal{T}_h} \left(\eta_{\mathrm{R}_2,K}^{n,k}\right)^2 (t)\, \mathrm{dt}\right\}^{\frac{1}{2}}. \tag{4.35}$$

Employing (4.34) and (4.35) we get the desired estimate. $\qquad\square$

Remark 4.9. *The estimators of Theorem 4.8 reflect various violations of physical properties of the approximate solution $v_{h\tau}^k$ and $w_{h\tau}^k$. The estimators $\eta_{\mathrm{R}_1,K}^{n,k}$ and $\eta_{\mathrm{F},K}^{n,k}$ represent the nonconformity of the flux, i.e. $\boldsymbol{\nabla} v_{h\tau}^k \notin \boldsymbol{H}(\mathrm{div}, \Omega)$. The term $\eta_{\mathrm{R}_2,K}^{n,k}$ is an estimator associated to the residual equation of the second line of (2.1). Indeed, $\partial_t w_{h\tau}^{n,k} + g(v_{h\tau}^{n,k}, w_{h\tau}^{n,k}) \neq 0$. However, at convergence ($k \to +\infty$, $h \to 0$ and $\Delta t_n \to 0$) all the estimators vanish showing that our methodology is consistent.*

5   Error components and adaptive algorithm

In Section 4, we derived an a posteriori error estimate between the exact solution and approximate solution at each time step $1 \leq n \leq N_t$, and at each Newton step $k \geq 1$ when $p \geq 1$. We now provide an a posteriori error estimate distinguishing the different error components, namely the error due to the discretization in space and the error due to the discretization in time. In particular, from the spatial error, we distinguish the discretization error stemming from the finite element method and the linearization error coming from the Newton scheme, following the heuristic approach presented in [24].

5.1 Space-time adaptivity

The flux estimator $\eta_{\mathrm{F},K}^{n,k}(t)$ is split into two contributions using the triangle inequality:

$$\eta_{\mathrm{F},K}^{n,k}(t) \le \left\| \Lambda \boldsymbol{\nabla} \left(v_{h\tau}^{n,k}(t) - v_h^{n,k} \right) \right\|_K + \left\| \Lambda \boldsymbol{\nabla} v_h^{n,k} + \boldsymbol{\sigma}_{h\tau,\mathrm{tot}}^{n,k} \right\|_K.$$

Using (4.1) we have $\forall t \in I_n$

$$v_{h\tau}^k(t) = \left(\frac{t - t^n}{\Delta t_n} + 1 \right) v_h^{n,k} - \frac{t - t^n}{\Delta t_n} v_h^{n-1} = (1 - \rho(t)) v_h^{n,k} + \rho(t) v_h^{n-1}$$

where $\rho(t) = \frac{t^n - t}{\Delta t_n}$. Furthermore, we have

$$\boldsymbol{\nabla} v_{h\tau}^k(t) = \boldsymbol{\nabla} v_h^{n,k} - \rho(t) \boldsymbol{\nabla}(v_h^{n,k} - v_h^{n-1}).$$

Therefore, we get

$$\eta_{\mathrm{F},K}^{n,k}(t) \le \rho(t) \left\| \Lambda \boldsymbol{\nabla}(v_h^{n,k} - v_h^{n-1}) \right\|_K + \left\| \Lambda \boldsymbol{\nabla} v_h^{n,k} + \boldsymbol{\sigma}_{h\tau,\mathrm{tot}}^{n,k} \right\|_K.$$

Nevertheless, the function $\rho : I_n \to \mathbb{R}$ is decreasing so that $\forall t \in I_n$, $\rho(t) \le \rho(t^{n-1}) = 1$. Therefore, we obtain

$$\eta_{\mathrm{F},K}^{n,k}(t) \le \underbrace{\left\| \Lambda \boldsymbol{\nabla}(v_h^{n,k} - v_h^{n-1}) \right\|_K}_{\eta_{\mathrm{tm},K}^{n,k}} + \underbrace{\left\| \Lambda \boldsymbol{\nabla} v_h^{n,k} + \boldsymbol{\sigma}_{h\tau,\mathrm{tot}}^{n,k} \right\|_K}_{\eta_{\mathrm{DF},K}^{n,k}}. \tag{5.1}$$

Corollary 5.1. *Let $\left(v_{h\tau}^k, w_{h\tau}^k \right)$ be the approximate solution issued from the exact linearization solver at each time step $1 \le n \le N_t$. Let $\boldsymbol{\sigma}_{h\tau,\mathrm{tot}}^k \in L^2(0, T; \boldsymbol{H}(\mathrm{div}, \Omega))$ be the equilibrated flux reconstruction satisfying (4.5). Consider the global estimator η^k of Theorem 4.8. Then, we obtain the following error estimate, distinguishing the two sources (spatial and temporal) of the error*

$$\eta^k \le \eta_{\mathrm{tm}}^k + \eta_{\mathrm{sp}}^k + \eta_{\mathrm{init}}^k$$

where

$$\eta_{\mathrm{sp}}^k = 2^{\frac{1}{2}} \left\{ \sum_{n=1}^{N_t} \int_{I_n} \sum_{K \in \mathcal{T}_h} \left(\eta_{\mathrm{R}_1,K}^{n,k} + \eta_{\mathrm{R}_2,K}^{n,k} + \eta_{\mathrm{DF},K}^{n,k} + \eta_{\mathrm{lin},1,K}^{n,k} \right)^2 (t) \, \mathrm{dt} \right\}^{\frac{1}{2}},$$

$$\eta_{\mathrm{tm}}^k = 2^{\frac{1}{2}} \left\{ \sum_{n=1}^{N_t} \int_{I_n} \sum_{K \in \mathcal{T}_h} \left(\eta_{\mathrm{tm},K}^{n,k} \right)^2 (t) \, \mathrm{dt} \right\}^{\frac{1}{2}},$$

$$\eta_{\mathrm{init}}^k := \left\{ \sum_{K \in \mathcal{T}_h} \left\{ \left(\eta_{\mathrm{IC},1,K}^k \right)^2 + \left(\eta_{\mathrm{IC},2,K}^k \right)^2 \right\} \right\}^{\frac{1}{2}}.$$

Proof. We first employ the inequality $A^2 + B^2 \le (A + B)^2 \ \forall (A, B) \in \mathbb{R}_+ \times \mathbb{R}_+$ to gather the residual estimators and we obtain

$$\eta^k \le \left\{ \sum_{n=1}^{N_t} \int_{I_n} \sum_{K \in \mathcal{T}_h} \left(\eta_{\mathrm{R}_1,K}^{n,k} + \eta_{\mathrm{R}_2,K}^{n,k} + \eta_{\mathrm{F},K}^{n,k} + \eta_{\mathrm{lin},1,K}^{n,k} \right)^2 (t) \, \mathrm{dt} \right.$$

$$\left. + \sum_{K \in \mathcal{T}_h} \left(\left(\eta_{\mathrm{IC},1,K}^k \right)^2 + \left(\eta_{\mathrm{IC},2,K}^k \right)^2 \right) \right\}^{\frac{1}{2}}.$$

Next, we use (5.1) to obtain

$$\eta^k \le \left\{ \sum_{n=1}^{N_t} \int_{I_n} \sum_{K \in \mathcal{T}_h} \left(\eta_{\mathrm{R}_1,K}^{n,k} + \eta_{\mathrm{R}_2,K}^{n,k} + \eta_{\mathrm{DF},K}^{n,k} + \eta_{\mathrm{tm},K}^{n,k} + \eta_{\mathrm{lin},1,K}^{n,k} \right)^2 (t) \, \mathrm{dt} \right.$$

$$\left. + \sum_{K \in \mathcal{T}_h} \left(\left(\eta_{\mathrm{IC},1,K}^k \right)^2 + \left(\eta_{\mathrm{IC},2,K}^k \right)^2 \right) \right\}^{\frac{1}{2}}.$$

19

The Minkowski inequality yields

$$\eta^k \leq \left\{ \left(\left\{ \sum_{n=1}^{N_t} \int_{I_n} \sum_{K \in \mathcal{T}_h} \left(\eta_{R_1,K}^{n,k} + \eta_{R_2,K}^{n,k} + \eta_{DF,K}^{n,k} + \eta_{lin,1,K}^{n,k} \right)^2 (t) \, dt \right\}^{\frac{1}{2}} \right. \right.$$
$$\left. + \left\{ \sum_{n=1}^{N_t} \int_{I_n} \sum_{K \in \mathcal{T}_h} (\eta_{tm,K}^{n,k})^2(t) \, dt \right\}^{\frac{1}{2}} \right)^2$$
$$\left. + \sum_{K \in \mathcal{T}_h} \left(\left(\eta_{IC,1,K}^{k} \right)^2 + \left(\eta_{IC,2,K}^{k} \right)^2 \right) \right\}^{\frac{1}{2}}.$$

Now, we employ the Cauchy–Schwarz inequality to get

$$\eta^k \leq \left\{ 2 \sum_{n=1}^{N_t} \int_{I_n} \sum_{K \in \mathcal{T}_h} \left(\eta_{R_1,K}^{n,k} + \eta_{R_2,K}^{n,k} + \eta_{DF,K}^{n,k} + \eta_{lin,1,K}^{n,k} \right)^2 (t) \, dt \right.$$
$$+ 2 \sum_{n=1}^{N_t} \int_{I_n} \sum_{K \in \mathcal{T}_h} (\eta_{tm,K}^{n,k})^2(t) \, dt$$
$$\left. + \sum_{K \in \mathcal{T}_h} \left(\left(\eta_{IC,1,K}^{k} \right)^2 + \left(\eta_{IC,2,K}^{k} \right)^2 \right) \right\}^{\frac{1}{2}}.$$

Finally, we get the desired result

$$\eta^k \leq 2^{\frac{1}{2}} \left\{ \sum_{n=1}^{N_t} \int_{I_n} \sum_{K \in \mathcal{T}_h} \left(\eta_{R_1,K}^{n,k} + \eta_{R_2,K}^{n,k} + \eta_{DF,K}^{n,k} + \eta_{lin,1,K}^{n,k} \right)^2 (t) \, dt \right\}^{\frac{1}{2}}$$
$$+ 2^{\frac{1}{2}} \left\{ \sum_{n=1}^{N_t} \int_{I_n} \sum_{K \in \mathcal{T}_h} \left(\eta_{tm,K}^{n,k} \right)^2 (t) \, dt \right\}^{\frac{1}{2}} + \left\{ \sum_{K \in \mathcal{T}_h} \left(\left(\eta_{IC,1,K}^{k} \right)^2 + \left(\eta_{IC,2,K}^{k} \right)^2 \right) \right\}^{\frac{1}{2}}.$$

$\square$

Remark 5.2. *The goal of an efficient numerical simulation is to achieve the equilibration of the spatial and temporal error components so that $\eta_{sp}^{n,k} \approx \eta_{tm}^{n,k} \; \forall 1 \leq n \leq N_t$ where $\eta_{sp}^{n,k} = \eta_{sp}^{k}|_{I_n}$ and $\eta_{tm}^{n,k} = \eta_{tm}^{k}|_{I_n}$ as well as the equilibration of the spatial error in all mesh elements $\eta_{sp,K'}^{n,k} \approx \eta_{sp,K}^{n,k}, \; \forall K' \neq K \in \mathcal{T}_h, \; \forall 1 \leq n \leq N_t$. This concept can be achieved thanks to an adaptive choice of the time step and mesh refinement procedures through algorithms such as those presented in Picasso [52], Makridakis and Nochetto [46], or Ern and Vohralík [31]. In this work, we mainly focus on the spatial component of the error. In the sequel, we present how to estimate the two spatial error components separately.*

5.2 Distinguishing the spatial-error components for $p \geq 1$

Let $1 \leq n \leq N_t$. First, we have $\boldsymbol{\sigma}_{h,tot}^{n,k} = \boldsymbol{\sigma}_{h,disc}^{n,k} + \boldsymbol{\sigma}_{h,lin}^{n,k}$ so the triangle inequality reads

$$\eta_{DF,K}^{n,k}(t) \leq \underbrace{\left\| \Lambda \boldsymbol{\nabla} v_h^{n,k} + \boldsymbol{\sigma}_{h\tau,disc}^{n,k} \right\|_K}_{\text{discretization}} + \underbrace{\left\| \boldsymbol{\sigma}_{h\tau,lin}^{n,k} \right\|_K}_{\text{linearization}}, \tag{5.2}$$

which separates the linearization and discretization contributions of the error. We then define

$$\eta_{FEM,K}^{n,k} := \left\| \Lambda \boldsymbol{\nabla} v_h^{n,k} + \boldsymbol{\sigma}_{h\tau,disc}^{n,k} \right\|_K, \quad \eta_{lin2,K}^{n,k} := \left\| \boldsymbol{\sigma}_{h\tau,lin}^{n,k} \right\|_K.$$

Thus, we can estimate separately the two contributions of the spatial error

Corollary 5.3. *Let $\left(v_{h\tau}^k, w_{h\tau}^k\right)$ be the approximate solution issued from the exact linearization solver at each time step $1 \leq n \leq N_{\mathrm{t}}$. Let $\boldsymbol{\sigma}_{h\tau,\mathrm{tot}}^k \in L^2(0,T; \boldsymbol{H}(\mathrm{div},\Omega))$ be the equilibrated flux reconstruction satisfying (4.5). Then, we get the following estimate distinguishing the two components (discretization and linearization) of the spatial error:*

$$\eta_{\mathrm{sp}}^k \leq \eta_{\mathrm{FEM}}^k + \eta_{\mathrm{lin}}^k$$

where

$$\eta_{\mathrm{FEM}}^k := 2^{\frac{1}{2}} \left\{ \sum_{n=1}^{N_t} \int_{I_n} \sum_{K \in \mathcal{T}_h} \left(\eta_{\mathrm{R}_1,K}^{n,k} + \eta_{\mathrm{R}_2,K}^{n,k} + \eta_{\mathrm{FEM},K}^{n,k} \right)^2 (t)\, \mathrm{d}t \right\}^{\frac{1}{2}},$$

$$\eta_{\mathrm{lin}}^k := 2^{\frac{1}{2}} \left\{ \sum_{n=1}^{N_t} \int_{I_n} \sum_{K \in \mathcal{T}_h} \left(\eta_{\mathrm{lin},1,K}^{n,k} + \eta_{\mathrm{lin},2,K}^{n,k} \right)^2 (t)\, \mathrm{d}t \right\}^{\frac{1}{2}}.$$

Proof. We use (5.2) and then the Minkowski inequality to obtain

$$\eta_{\mathrm{sp}}^k = 2^{\frac{1}{2}} \left\{ \sum_{n=1}^{N_t} \int_{I_n} \sum_{K \in \mathcal{T}_h} \left(\eta_{\mathrm{R}_1,K}^{n,k} + \eta_{\mathrm{R}_2,K}^{n,k} + \eta_{\mathrm{DF},K}^{n,k} + \eta_{\mathrm{lin},1,K}^{n,k} \right)^2 (t)\, \mathrm{d}t \right\}^{\frac{1}{2}}$$

$$\leq 2^{\frac{1}{2}} \left\{ \sum_{n=1}^{N_t} \int_{I_n} \sum_{K \in \mathcal{T}_h} \left(\eta_{\mathrm{R}_1,K}^{n,k} + \eta_{\mathrm{R}_2,K}^{n,k} + \eta_{\mathrm{FEM},K}^{n,k} + \eta_{\mathrm{lin},1,K}^{n,k} + \eta_{\mathrm{lin},2,K}^{n,k} \right)^2 (t)\, \mathrm{d}t \right\}^{\frac{1}{2}}$$

$$\leq 2^{\frac{1}{2}} \left\{ \sum_{n=1}^{N_t} \int_{I_n} \sum_{K \in \mathcal{T}_h} \left(\eta_{\mathrm{R}_1,K}^{n,k} + \eta_{\mathrm{R}_2,K}^{n,k} + \eta_{\mathrm{FEM},K}^{n,k} \right)^2 (t)\, \mathrm{d}t \right\}^{\frac{1}{2}}$$

$$+ 2^{\frac{1}{2}} \left\{ \sum_{n=1}^{N_t} \int_{I_n} \sum_{K \in \mathcal{T}_h} \left(\eta_{\mathrm{lin},1,K}^{n,k} + \eta_{\mathrm{lin},2,K}^{n,k} \right)^2 (t)\, \mathrm{d}t \right\}^{\frac{1}{2}}.$$

$\square$

Combining the previous results, we get the a posteriori error estimate distinguishing the different error components

Corollary 5.4. *Let $\left(v_{h\tau}^k, w_{h\tau}^k\right)$ be the approximate solution issued from the exact linearization solver at each time step $1 \leq n \leq N_{\mathrm{t}}$. Then, we get the following error estimate, distinguishing the different error components*

$$\eta^k \leq \eta_{\mathrm{tm}}^k + \eta_{\mathrm{FEM}}^k + \eta_{\mathrm{lin}}^k + \eta_{\mathrm{init}}^k.$$

Remark 5.5. *The estimators defined in Corollary 5.4 are global. Their local versions are defined by*

$$\eta_{\mathrm{FEM}}^{n,k} := 2^{\frac{1}{2}} \left\{ \int_{I_n} \sum_{K \in \mathcal{T}_h} \left(\eta_{\mathrm{R}_1,K}^{n,k} + \eta_{\mathrm{R}_2,K}^{n,k} + \eta_{\mathrm{FEM},K}^{n,k} \right)^2 (t)\, \mathrm{d}t \right\}^{\frac{1}{2}},$$

$$\eta_{\mathrm{lin}}^{n,k} := 2^{\frac{1}{2}} \left\{ \int_{I_n} \sum_{K \in \mathcal{T}_h} \left(\eta_{\mathrm{lin},1,K}^{n,k} + \eta_{\mathrm{lin},2,K}^{n,k} \right)^2 (t)\, \mathrm{d}t \right\}^{\frac{1}{2}},$$

$$\eta_{\mathrm{tm}}^{n,k} := 2^{\frac{1}{2}} \left\{ \int_{I_n} \sum_{K \in \mathcal{T}_h} \left(\eta_{\mathrm{tm},K}^{n,k} \right)^2 (t)\, \mathrm{d}t \right\}^{\frac{1}{2}}.$$

Remark 5.6. *Note that the total discretization error estimator has two components: the first one comes from the finite element method, and the second one stems from the Newton linearization procedure. Therefore, the total discretization estimator is a combination of η_{FEM}^k and η_{tm}^k. More precisely one has*

$$\eta_{\mathrm{FEM}}^k + \eta_{\mathrm{tm}}^k \leq \eta_{\mathrm{disc}}^k := 2^{\frac{1}{2}} \left\{ \sum_{n=1}^{N_t} \left(\left(\eta_{\mathrm{FEM}}^{n,k} \right)^2 + \left(\eta_{\mathrm{tm}}^{n,k} \right)^2 \right) (t)\, \mathrm{d}t \right\}^{\frac{1}{2}}$$

so that its local-in-time version reads

$$\eta_{\mathrm{disc}}^{n,k} := 2^{\frac{1}{2}} \left\{ \left(\eta_{\mathrm{FEM}}^{n,k} \right)^2 + \left(\eta_{\mathrm{tm}}^{n,k} \right)^2 \right\}^{\frac{1}{2}}.$$

5.3 Adaptive Newton algorithm

We finally present our adaptive Newton algorithm. Following the concept of [24, 32], it is designed only to perform the linearization resolution with minimal necessary precision, and thus to avoid unnecessary iterations. Let γ_{lin} be a positive parameter, typically of order 0.1, representing the desired relative size of the linearization error. Assuming that the initial estimator η_{init} is negligible, we summarize it in Algorithm 1.

Algorithm 1 Adaptive Newton algorithm at each time step $n \geq 1$

1. Choose an initial vector $\boldsymbol{X}_h^{n,0} \in \mathbb{R}^{2\mathcal{N}_d^p}$, typically as $\boldsymbol{X}_h^{n-1}$, and set $k = 1$.
2. From $\boldsymbol{X}_h^{n,k-1}$ define $\mathbb{A}^{n,k-1} \in \mathbb{R}^{2\mathcal{N}_d^p, 2\mathcal{N}_d^p}$ and $\boldsymbol{B}^{n,k-1} \in \mathbb{R}^{2\mathcal{N}_d^p}$ by (3.12).
3. Consider the linear system

$$\mathbb{A}^{n,k-1} \boldsymbol{X}_h^{n,k} = \boldsymbol{B}^{n,k-1}.$$

4. Compute the estimators of Theorem 4.8 and check the stopping criterion for the linear solver in the form:
$$\eta_{\mathrm{lin}}^{n,k} \leq \gamma_{\mathrm{lin}} \eta_{\mathrm{disc}}^{n,k}. \tag{5.3}$$
If satisfied, return $\boldsymbol{X}_h^n = \boldsymbol{X}_h^{n,k}$. If not, set $k = k+1$ and go back to **1**.

---

6 Numerical experiments

This section illustrates numerically our theoretical developments in the case of linear $p = 1$. We first assume that the Newton solver has converged, i.e., we apply the "exact Newton" method as described in Section 3.3, using the stopping criterion with $\varepsilon = 10^{-12}$. In this scenario, the Newton index k can be discarded. Let $\Omega := [-1, 1] \times [-1, 1]$ denotes the unit square. In a first study, we are interested in the shape of the numerical solution after several time steps and in the behavior of the estimators at convergence of the solvers given by Theorem 4.8. We recall that in this scenario, the linearization estimators vanish, so that it will not be represented in our figures. In a second study, we will focus on our adaptive Newton strategy given by Algorithm 1. For all the studies, the initial conditions are given by

$$v_0(\boldsymbol{x}) = 0.3, \text{ and } w_0(\boldsymbol{x}) = 0.$$

Furthermore, the simulations are conducted under the assumption of an isotropic tissue structure, with a conductivity tensor $\Lambda := \begin{pmatrix} 2 & 1 \\ 1 & 2 \end{pmatrix}$. We take a constant time step $\Delta t_n = \Delta t = 0.1$ for all $1 \leq n \leq N_{\mathrm{t}} = 2000$, and the final time of simulation is $T = 200$. For modeling ionic current flows, we employ the original FitzHugh–Nagumo model [36, 49], with parameter values given by $\lambda = 1$, $\theta = 0.25$, $a = 0.005$, and $b = 0.025$. The discrete initial conditions are chosen such that $v_h^0(\boldsymbol{x}) = v_0(\boldsymbol{x})$ and $w_h^0(\boldsymbol{x}) = w_0(\boldsymbol{x})$. Obviously, the initial condition estimators given by (4.29) vanish.

6.1 Exact Newton method at convergence

In this section, the Newton algorithm has converged, and we employ the stopping criterion (3.13) with $\varepsilon = 10^{-12}$. Figure 1 illustrates the temporal evolution of the transmembrane potential v_h and the recovery variable w_h as functions of the time step, in the case where the Newton solver has converged. The transmembrane potential v_h (blue curve) represents the electrical activation of a cardiac cell, whereas the recovery variable w_h (red curve) accounts for the delayed response of ionic channels, such as potassium (K^+)
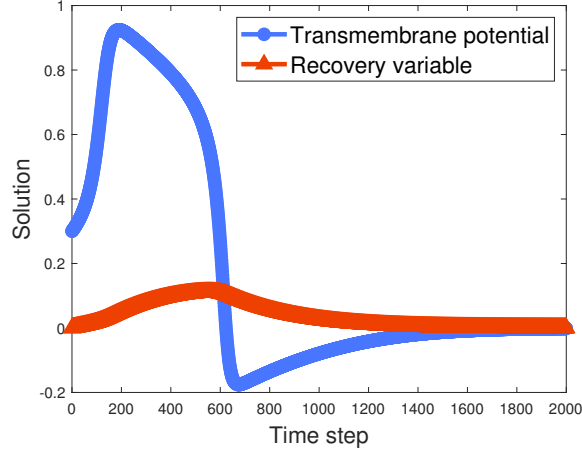
Figure 1: Temporal evolution of the exact numerical solution (v_h^n, w_h^n) at a fixed spatial point, computed for 15130 mesh elements.

and sodium (Na^+) channels. The overall dynamics can be divided into three main phases. First, during the *rapid depolarization* phase, the membrane potential v_h increases rapidly due to the sudden opening of sodium channels. It exceeds a critical threshold ($\theta = 0.25$) and increases rapidly, while w_h responds more slowly to this excitation. Then, in the *repolarization* phase, the variable w_h grows large enough to inhibit the dynamics of v_h, which begins to decrease. This corresponds to the closure of sodium channels and the delayed opening of potassium channels, leading to an efflux of K^+ ions and a consequent drop in transmembrane potential. Finally, during the *return to the resting state* phase, both v_h and w_h gradually return to their baseline values ($v_h = w_h = 0$). This recovery process is supported by the closure of potassium channels and the activity of ionic pumps, such as the Na^+/K^+-ATPase, which helps restore ionic balance by actively transporting Na^+ ions out of the cell and K^+ ions in. The resulting trajectories highlight the coupled nature of excitation and recovery mechanisms during the signal propagation.
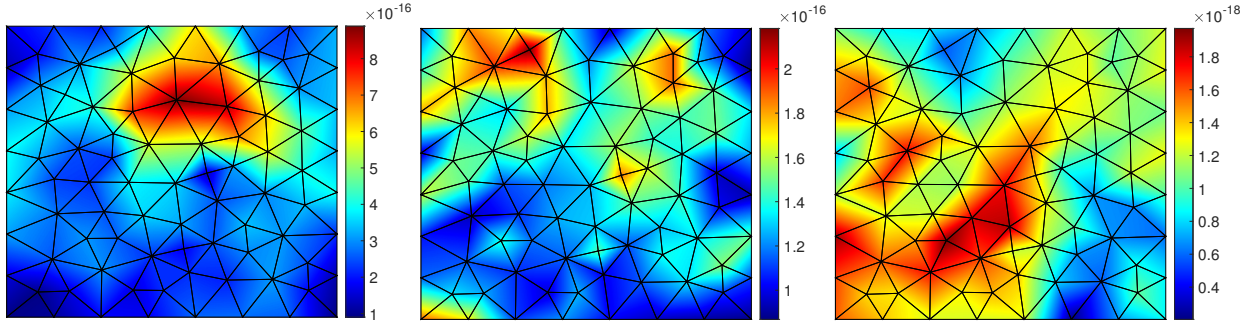
Figure 2: Estimators at convergence for approximately 148 elements at time value $t_n = 20$. Left: flux estimator $\eta_{\mathrm{F},K}^n$. Middle and right: residual estimators $\eta_{\mathrm{R}_1,K}^n$ and $\eta_{\mathrm{R}_2,K}^n$, respectively.

Figures 2 and 3 display the behavior of the flux estimator $\eta_{\mathrm{F},K}^n(t_n)$ (4.27) and of the residual estimators $\eta_{\mathrm{R}_1,K}^n(t_n)$ and $\eta_{\mathrm{R}_2,K}^n(t_n)$ (4.26) (see Theorem 4.8) associated to the transmembrane potential v_h^n and the recovery variable w_h^n at the time value $t_n = 20$, for two different meshes. We observe that for several spatial meshes, these discretization estimators are very small. It in particular shows that when the Newton solver has converged the numerical flux $\boldsymbol{\nabla} v_{h\tau}^{n,k}$ is almost conforming since it is very close in the sense of the L^2 norm to the equilibrated flux $\boldsymbol{\sigma}_{h\tau,\mathrm{tot}}^{n,k} \in \mathbf{H}(\mathrm{div}, \Omega)$. Obviously, this amazing phenomenon does not occur within the Newton iteration. Thus, our finite element method produces a high-fidelity numerical solution that recovers the structural properties of the solution at the continuous level.
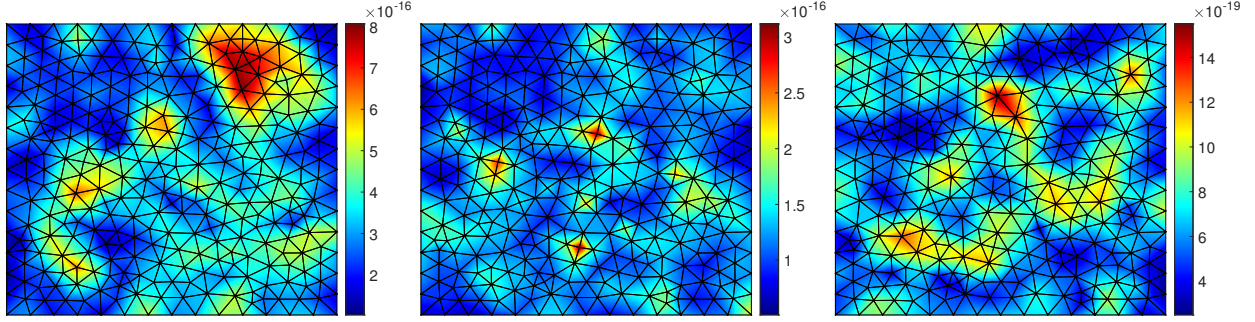
Figure 3: Estimators at convergence for approximately 600 elements at time value $t_n = 20$. Left: flux estimator $\eta_{\mathrm{F},K}^n$. Middle and right: residual estimators $\eta_{\mathrm{R}_1,K}^n$ and $\eta_{\mathrm{R}_2,K}^n$, respectively.
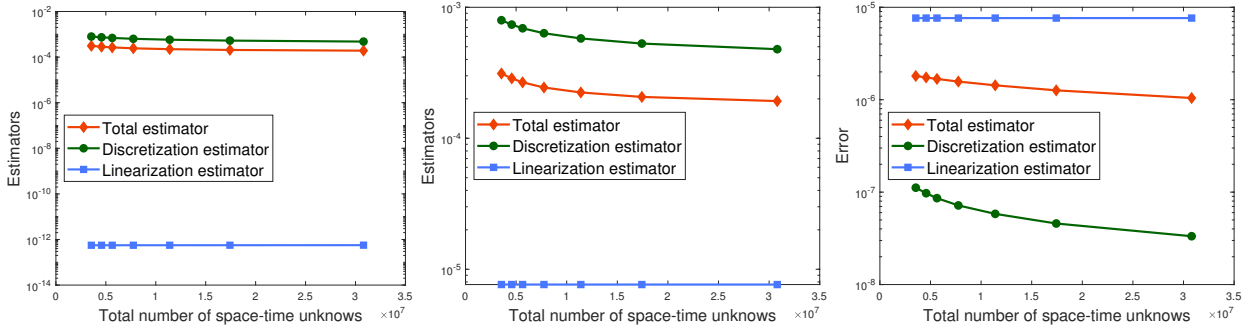

Figure 4: *A posteriori* estimators η^k, η_{disc}^k, and η_{lin}^k at convergence, as a function of the total number of space-time unknowns. Exact Newton method (left); adaptive Newton method (middle); error between the two approaches (right).

6.2 Comparison of exact and adaptive Newton algorithm

Figure 4 displays the curves of the different global estimators as a function of the total number of space-time unknowns. More precisely, if we denote by $|\mathcal{T}_h|$ the total number of elements composing the mesh $\mathcal{T}_h$, then the total number of space-time unknowns is $N_\mathrm{t} \times |\mathcal{T}_h|$. Therefore, the x-axis represents a sequence of values corresponding to different mesh refinements. In the left part of Figure 4, the Newton stopping criterion (3.13) is satisfied, while in the middle one, the adaptive stopping criterion (5.3) is applied. In both cases, the total estimator η^k defined by (4.30) (red curve) is nearly identical, indicating that the adaptive method achieves comparable accuracy to the exact Newton method. In fact, the discretization estimator η_{disc}^k (green curve) is dominant, with values around 10^{-3} in both configurations (the right figure confirms that both curves are quite similar). In the exact case, the linearization estimator η_{lin}^k (blue curve) is extremely small (around 10^{-12}). On the other hand, in the adaptive case, the linearization estimator takes slightly larger values (around 10^{-6}), which however remain small enough not to affect the overall estimator. Note that the right part of Figure 4 depicts the errors between each methods for each estimators. It enables us to show clearly the deviation between the two approaches.

Figure 5 presents the evolution of the various estimators as a function of the Newton iterations at three time values $t_n = 116$, $t_n = 144$, and $t_n = 200$. We observe that the discretization estimator globally dominates and is close to the total estimator. The linearization estimator (blue curve) is small from the second Newton iteration (around 10^{-2}) and next decreases rapidly to reach the value 10^{-15}. From the first Newton iteration, the discretization estimator stagnates, which means that the linearization component of the error does not influence the behavior of the total error estimator. Then, the Newton algorithm performs unnecessary iterations and could be stopped after the second iteration. Here again, we highlight an interesting observation: the linearization estimator and the Newton error exhibit similar behavior, up to a small constant shift. This result confirms the consistency of our heuristic approach in separating the different error components from the total estimator.

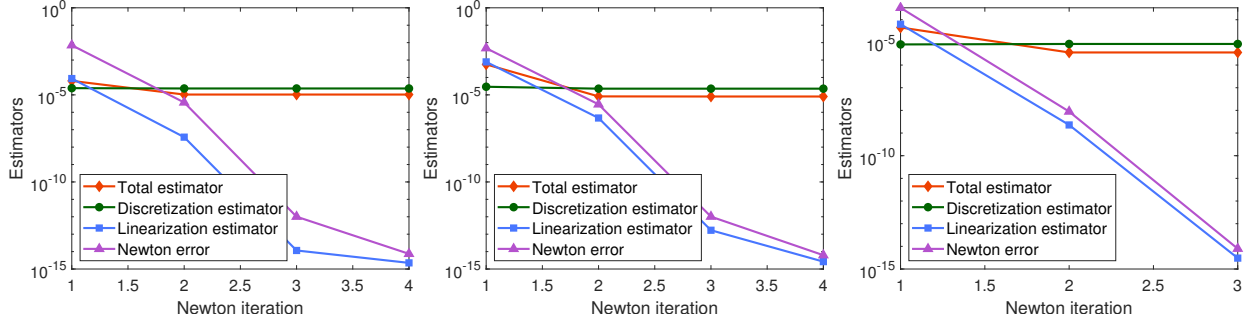Figure 6 shows the number of Newton iterations and the cumulative number of Newton iterations required

Figure 5: Estimators as a function of the Newton iterations for three different time steps: $t_n = 116$, $t_n = 144$, and $t_n = 200$.
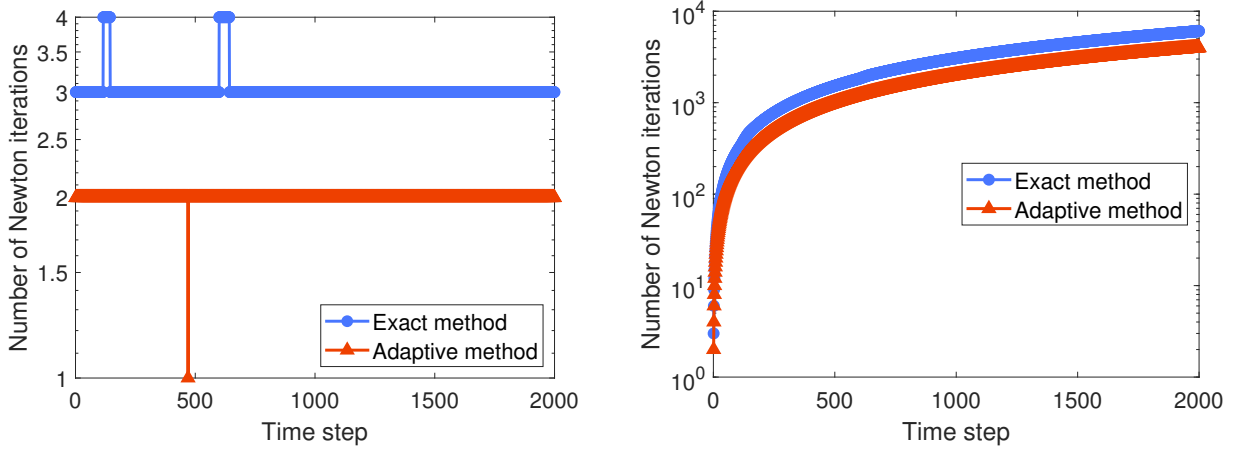

Figure 6: Left: number of Newton iterations at each time step. Right: cumulated number of Newton iterations as a function of time.

to meet the stopping criteria at each time step of the simulation. In particular, the first plot shows that, for almost all time steps, our adaptive strategy requires only 2 Newton iterations to converge and is cheaper in terms of Newton iterations than the exact resolution. The second graph presents the cumulated number of Newton iterations as a function of time step. A clear advantage of the adaptive Newton approach can be observed, as it reduces the total number of iterations by approximately 35% by the end of the simulation.

Figure 7 (left) displays the evolution of the adaptive numerical solution as a function of the time step. The second graph illustrates the error between the solutions given by the exact (recall Figure 1) resolution and the adaptive one. In particular, the curves of the solutions given by exact Newton and adaptive Newton almost coincide. Thus, our adaptive Newton algorithm saves many Newton iterations and generates a solution whose precision does not differ from the exact one more than by a fraction of the discretization error.

Figure 8 displays the behavior of the spatial estimator η_{sp}^k and the temporal estimator η_{tm}^k of Corollary 5.1 for several space-time meshes. We observe in both figures that the temporal estimator is very small, indicating that the error stemming from the implicit Euler scheme is also small. This result is coherent and explained by the fact that the numerical solution evolves very slowly over time. Next, we observe a small fluctuation of the spatial estimator between the two methods. The spatial estimator is obviously higher than the temporal estimator since it concentrates the main source of the error. It gives important tools for adaptive space-time mesh refinement strategies where an equilibrium between the spatial error and temporal error is sought. It will be considered in a future work.
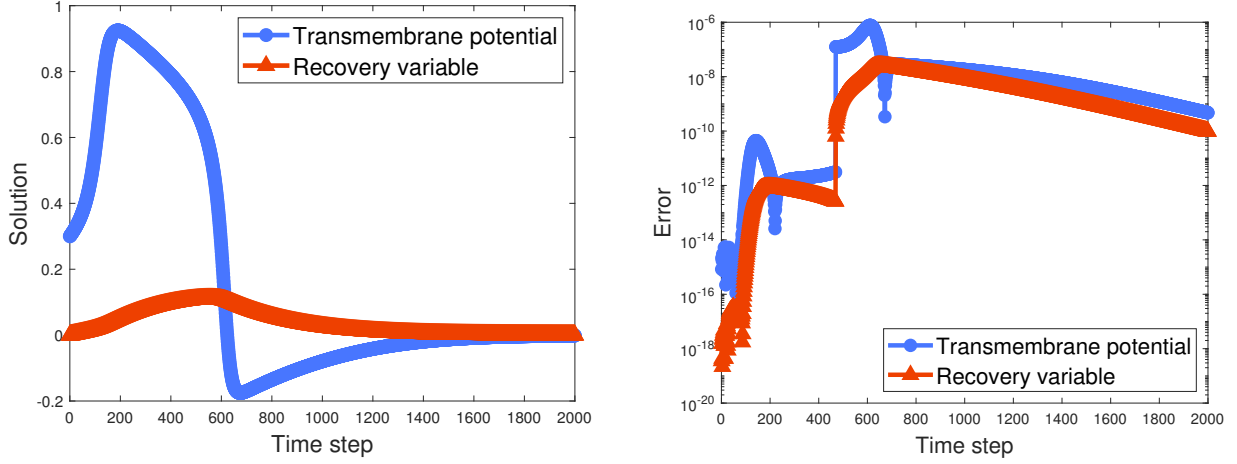
25

Figure 7: Left: temporal evolution of the adaptive numerical solution (v_h^n, w_h^n) at a fixed spatial point at convergence. Right: error between the exact and adaptive methods.
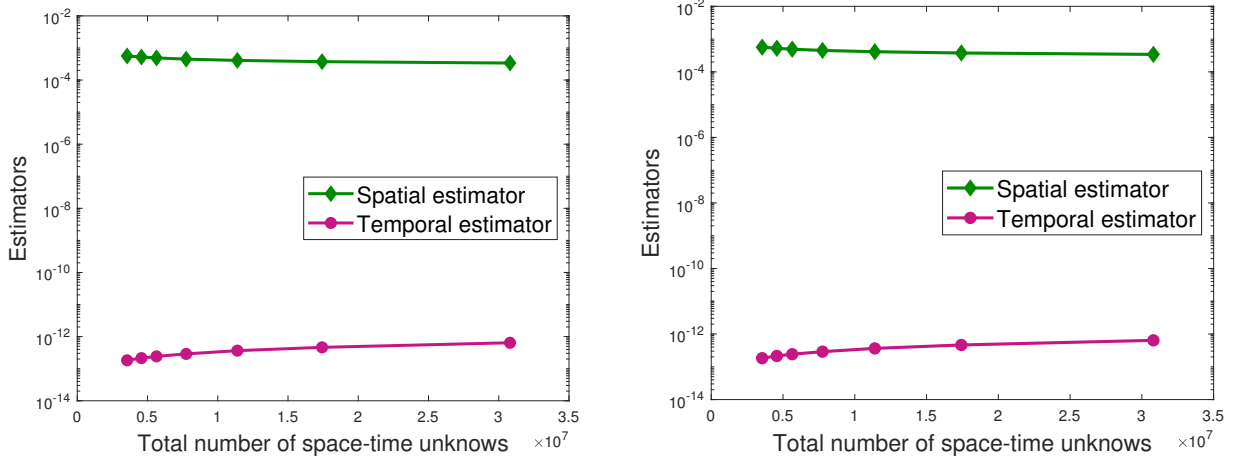

Figure 8: Spatial η_{sp}^k and temporal η_{tm}^k estimators as a function of the total number of space–time unknowns. Exact (left) and adaptive (right) Newton method.

7 Conclusion

In this work, we devised an adaptive version of the Newton algorithm for the monodomain problem in electrocardiology. We employed the conforming $\mathbb{P}_p$ finite element method for spatial discretization and the implicit Euler scheme for time discretization. Using equilibrated flux reconstructions, we established an *a posteriori* error estimate on the error between the exact and approximate solutions, which is valid at each time step and each Newton iteration. Our *a posteriori* error estimate also distinguishes — through a heuristic approach — the main component of the error (spatial error), which is splitted into two contributions: the discretization error and the linearization error. This distinction of error components enabled us to formulate an adaptive stopping criterion for the linearization solver in order to reduce the computational cost. In the numerical experiments, we tested the effectiveness of our adaptive strategy. In particular, the results confirmed the robustness of the proposed approach.

Acknowledgments

References

[1] G. Acosta and R. Durán, *An optimal poincaré inequality in l^1 for convex domains*, Proceedings of the american mathematical society, 132 (2004), pp. 195–202.

[2] M. Ainsworth and J. T. Oden, *A posteriori error estimation in finite element analysis*, Pure and Applied Mathematics (New York), Wiley-Interscience [John Wiley & Sons], New York, 2000.

[3] R. R. Aliev and A. V. Panfilov, *A simple two-variable model of cardiac excitation*, Chaos, Solitons & Fractals, 7 (1996), pp. 293–301.

[4] L. Ambrosio, P. Colli Franzone, and G. Savaré, *On the asymptotic behaviour of anisotropic energies arising in the cardiac bidomain model*, Interfaces Free Bound., 2 (2000), pp. 213–266.

[5] D. N. Arnold, *An interior penalty finite element method with discontinuous elements*, SIAM J. Numer. Anal., 19 (1982), pp. 742–760.

[6] C. J. Arthurs, M. J. Bishop, and D. Kay, *Efficient simulation of cardiac electrical propagation using high order finite elements*, J. Comput. Phys., 231 (2012), pp. 3946–3962.

[7] F. Bader, M. Bendahmane, M. Saad, and R. Talhouk, *Derivation of a new macroscopic bidomain model including three scales for the electrical activity of cardiac tissue*, J. Engrg. Math., 131 (2021), pp. Paper No. 3, 30.

[8] ———, *Three scale unfolding homogenization method applied to cardiac bidomain model*, Acta Appl. Math., 176 (2021), pp. Paper No. 14, 37.

[9] ———, *Microscopic tridomain model of electrical activity in the heart with dynamical gap junctions. Part 1—Modeling and well-posedness*, Acta Appl. Math., 179 (2022), pp. Paper No. 11, 35.

[10] ———, *Microscopic tridomain model of electrical activity in the heart with dynamical gap junctions. Part 2—Derivation of the macroscopic tridomain model by unfolding homogenization method*, Asymptot. Anal., 132 (2023), pp. 575–606.

[11] R. Becker, C. Johnson, and R. Rannacher, *Adaptive error control for multigrid finite element methods*, Computing, 55 (1995), pp. 271–288.

[12] G. W. Beeler and H. Reuter, *Reconstruction of the action potential of ventricular myocardial fibres*, The Journal of physiology, 268 (1977), pp. 177–210.

[13] A. Bergam, C. Bernardi, and Z. Mghazli, *A posteriori analysis of the finite element discretization of some parabolic equations*, Math. Comp., 74 (2005), pp. 1117–1138.

[14] C. Bernardi, Y. Maday, and F. Rapetti, *Discrétisations variationnelles de problèmes aux limites elliptiques*, vol. 45 of Mathématiques & Applications (Berlin) [Mathematics & Applications], Springer-Verlag, Berlin, 2004.

[15] Y. Bourgault, Y. Coudière, and C. Pierre, *Existence and uniqeness of the solution for the bidomain model used in cardiac electrophysiology*, Nonlinear Anal. Real World Appl., 10 (2009), pp. 458–482.

[16] D. Braess, V. Pillwein, and J. Schöberl, *Equilibrated residual error estimates are p-robust*, Comput. Methods Appl. Mech. Engrg., 198 (2009), pp. 1189–1197.

[17] J. H. Bramble and S. R. Hilbert, *Estimation of linear functionals on Sobolev spaces with application to Fourier transforms and spline interpolation*, SIAM J. Numer. Anal., 7 (1970), pp. 112–124.

[18] S. C. Brenner and L. R. Scott, *The mathematical theory of finite element methods*, vol. 15 of Texts in Applied Mathematics, Springer-Verlag, New York, 1994.

[19] J. Céa, *Approximation variationnelle des problèmes aux limites*, Ann. Inst. Fourier (Grenoble), 14 (1964), pp. 345–444.

[20] S. Chellappa, B. s. Cansi z, L. Feng, P. Benner, and M. Kaliske, *Fast and reliable reduced-order models for cardiac electrophysiology*, GAMM-Mitt., 46 (2023), pp. Paper No. e202370014, 25.

[21] P. Colli Franzone, P. Deuflhard, B. Erdmann, J. Lang, and L. F. Pavarino, *Adaptivity in space and time for reaction-diffusion systems in electrocardiology*, SIAM J. Sci. Comput., 28 (2006), pp. 942–962.

[22] P. Colli Franzone, L. F. Pavarino, and B. Taccardi, *Simulating patterns of excitation, repolarization and action potential duration with cardiac bidomain and monodomain models*, Math. Biosci., 197 (2005), pp. 35–66.

[23] J. Dabaghi and G. Delay, *A unified framework for high-order numerical discretizations of variational inequalities*, Comput. Math. Appl., 92 (2021), pp. 62–75.

[24] J. Dabaghi, V. Martin, and M. Vohralík, *Adaptive Inexact Semismooth Newton Methods for the Contact Problem Between Two Membranes*, J. Sci. Comput., 84 (2020), p. 28.

[25] ——, *A posteriori estimates distinguishing the error components and adaptive stopping criteria for numerical approximations of parabolic variational inequalities*, Comput. Methods Appl. Mech. Engrg., 367 (2020), p. 113105.

[26] P. Destuynder and B. Métivet, *Explicit error bounds in a conforming finite element method*, Math. Comp., 68 (1999), pp. 1379–1396.

[27] P. Deuflhard, *Cascadic conjugate gradient methods for elliptic partial differential equations: algorithm and numerical results*, in Domain decomposition methods in scientific and engineering computing (University Park, PA, 1993), vol. 180 of Contemp. Math., Amer. Math. Soc., Providence, RI, 1994, pp. 29–42.

[28] D. A. Di Pietro and A. Ern, *Mathematical aspects of discontinuous Galerkin methods*, vol. 69 of Mathématiques & Applications (Berlin) [Mathematics & Applications], Springer, Heidelberg, 2012.

[29] D. A. Di Pietro, A. Ern, and S. Lemaire, *An arbitrary-order and compact-stencil discretization of diffusion on general meshes based on local reconstruction operators*, Comput. Methods Appl. Math., 14 (2014), pp. 461–472.

[30] A. Ern, I. Smears, and M. Vohralík, *Guaranteed, locally space-time efficient, and polynomial-degree robust a posteriori error estimates for high-order discretizations of parabolic problems*, SIAM J. Numer. Anal., 55 (2017), pp. 2811–2834.

[31] A. Ern and M. Vohralík, *A posteriori error estimation based on potential and flux reconstruction for the heat equation*, SIAM J. Numer. Anal., 48 (2010), pp. 198–223.

[32] A. Ern and M. Vohralík, *Adaptive inexact Newton methods with a posteriori stopping criteria for nonlinear diffusion PDEs*, SIAM J. Sci. Comput., 35 (2013), pp. A1761–A1791.

[33] L. C. Evans, *Partial differential equations*, vol. 19 of Graduate Studies in Mathematics, American Mathematical Society, 1997.

[34] R. Eymard, T. Gallouët, and R. Herbin, *Convergence of finite volume schemes for semilinear convection diffusion equations*, Numer. Math., 82 (1999), pp. 91–116.

[35] R. Eymard, R. Herbin, and A. Michel, *Mathematical study of a petroleum-engineering scheme*, M2AN Math. Model. Numer. Anal., 37 (2003), pp. 937–972.

[36] R. FitzHugh, *Impulses and physiological states in theoretical models of nerve membrane*, Biophysical journal, 1 (1961), pp. 445–466.

[37] P. C. Franzone, L. Pavarino, and B. Taccardi, *Simulating patterns of excitation, repolarization and action potential duration with cardiac bidomain and monodomain models*, Mathematical biosciences, 197 (2005), pp. 35–66.

[38] I. B. Gharbia, J. Dabaghi, V. Martin, and M. Vohralík, *A posteriori error estimates for a compositional two-phase flow with nonlinear complementarity constraints*, Comput. Geosci., 24 (2020), pp. 1031–1055.

[39] C. S. Henriquez and W. Ying, *The bidomain model of cardiac tissue: from microscale to macroscale*, in Cardiac Bioelectric Therapy, Springer, 2009, pp. 401–421.

[40] A. L. Hodgkin and A. F. Huxley, *A quantitative description of membrane current and its application to conduction and excitation in nerve*, The Journal of physiology, 117 (1952), pp. 500–544.

[41] R. Huber and R. Helmig, *Node-centered finite volume discretizations for the numerical simulation of multiphase flow in heterogeneous porous media*, Comput. Geosci., 4 (2000), pp. 141–164.

[42] K. H. Jæger, A. G. Edwards, A. McCulloch, and A. Tveito, *Properties of cardiac conduction in a cell-based computational model*, PLoS computational biology, 15 (2019), p. e1007042.

[43] J. P. Keener and J. Sneyd, *Mathematical physiology*, vol. 1, Springer, 1998.

[44] L. P. Lindner, T. Gerach, T. Jahnke, A. Loewe, D. Weiss, and C. Wieners, *Efficient time splitting schemes for the monodomain equation in cardiac electrophysiology*, International Journal for Numerical Methods in Biomedical Engineering, 39 (2023), p. e3666.

[45] C.-h. Luo and Y. Rudy, *A dynamic model of the cardiac ventricular action potential. i. simulations of ionic currents and concentration changes.*, Circulation research, 74 (1994), pp. 1071–1096.

[46] C. Makridakis and R. H. Nochetto, *Elliptic reconstruction and a posteriori error estimates for parabolic problems*, SIAM J. Numer. Anal., 41 (2003), pp. 1585–1594.

[47] L. Mirabella, F. Nobile, and A. Veneziani, *An a posteriori error estimator for model adaptivity in electrocardiology*, Comput. Methods Appl. Mech. Engrg., 200 (2011), pp. 2727–2737.

[48] C. C. Mitchell and D. G. Schaeffer, *A two-current model for the dynamics of cardiac membrane*, Bulletin of mathematical biology, 65 (2003), pp. 767–793.

[49] J. Nagumo, S. Arimoto, and S. Yoshizawa, *An active pulse transmission line simulating nerve axon*, Proceedings of the IRE, 50 (1962), pp. 2061–2070.

[50] P. Pathmanathan, G. R. Mirams, J. Southern, and J. P. Whiteley, *The significant effect of the choice of ionic current integration method in cardiac electro-physiological simulations*, Int. J. Numer. Methods Biomed. Eng., 27 (2011), pp. 1751–1770.

[51] S. Pezzuto, J. Hake, and J. Sundnes, *Space-discretization error analysis and stabilization schemes for conduction velocity in cardiac electrophysiology*, Int. J. Numer. Methods Biomed. Eng., 32 (2016), pp. e02762, 26.

[52] M. Picasso, *Adaptive finite elements for a linear parabolic problem*, Comput. Methods Appl. Mech. Engrg., 167 (1998), pp. 223–237.

[53] Z. Qu and A. Garfinkel, *An advanced algorithm for solving partial differential equation in cardiac conduction*, IEEE transactions on biomedical engineering, 46 (1999), pp. 1166–1168.

[54] A. Quarteroni and A. Valli, *Numerical approximation of partial differential equations*, vol. 23 of Springer Series in Computational Mathematics, Springer-Verlag, Berlin, 1994.

[55] L. Ratti and M. Verani, *A posteriori error estimates for the monodomain model in cardiac electrophysiology*, Calcolo, 56 (2019), pp. Paper No. 33, 33.

[56] S. Repin, *A posteriori estimates for partial differential equations*, vol. 4 of Radon Series on Computational and Applied Mathematics, Walter de Gruyter GmbH & Co. KG, Berlin, 2008.

[57] B. Rivière, *Discontinuous Galerkin methods for solving elliptic and parabolic equations*, vol. 35 of Frontiers in Applied Mathematics, Society for Industrial and Applied Mathematics (SIAM), Philadelphia, PA, 2008. Theory and implementation.

[58] J. M. Rogers and A. D. McCulloch, *A collocation-galerkin finite element model of cardiac action potential propagation*, IEEE Transactions on Biomedical Engineering, 41 (1994), pp. 743–757.

[59] G. Rosilho de Souza, M. J. Grote, S. Pezzuto, and R. Krause, *Explicit stabilized multirate methods for the monodomain model in cardiac electrophysiology*, ESAIM Math. Model. Numer. Anal., 58 (2024), pp. 2225–2254.

[60] S. Sanfelici, *Convergence of the Galerkin approximation of a degenerate evolution problem in electrocardiology*, Numer. Methods Partial Differential Equations, 18 (2002), pp. 218–240.

[61] O. H. Schmitt, *Biological information processing using the concept of interpenetrating domains*, in Information Processing in The Nervous System: Proceedings of a Symposium held at the State University of New York at Buffalo 21st–24th October, 1968, Springer, 1969, pp. 325–331.

[62] G. Strang, *The finite element method and approximation theory*, in Numerical Solution of Partial Differential Equations, II (SYNSPADE 1970) (Proc. Sympos., Univ. of Maryland, College Park, Md., 1970), Academic Press, New York, 1971, pp. 547–583.

[63] J. Sundnes, G. T. Lines, X. Cai, B. r. F. Nielsen, K.-A. Mardal, and A. Tveito, *Computing the electrical activity in the heart*, vol. 1 of Monographs in Computational Science and Engineering, Springer-Verlag, Berlin, 2006.

[64] J. Sundnes, G. T. Lines, and A. Tveito, *An operator splitting method for solving the bidomain equations coupled to a volume conductor model for the torso*, Math. Biosci., 194 (2005), pp. 233–248.

[65] J. Sundnes, B. F. Nielsen, K. A. Mardal, X. Cai, G. T. Lines, and A. Tveito, *On the computational complexity of the bidomain and the monodomain models of electrophysiology*, Annals of biomedical engineering, 34 (2006), pp. 1088–1097.

[66] L. Tung, *A bi-domain model for describing ischemic myocardial dc potentials.*, PhD thesis, Massachusetts Institute of Technology, 1978.

[67] A. Tveito, K. H. Jæger, M. Kuchta, K.-A. Mardal, and M. E. Rognes, *A cell-based framework for numerical modeling of electrical conduction in cardiac tissue*, Frontiers in Physics, 5 (2017), p. 48.

[68] R. Verfürth, *A posteriori error estimates for nonlinear problems: $L^r(0,T;W^{1,\rho}(\Omega))$-error estimates for finite element discretizations of parabolic equations*, Numer. Methods Partial Differential Equations, 14 (1998), pp. 487–518.

[69] R. Verfürth, *A posteriori error estimation techniques for finite element methods*, Numerical Mathematics and Scientific Computation, Oxford University Press, Oxford, 2013.